

A multiphase phase-field study of three-dimensional martensitic twinned microstructures at large strains

Anup Basak¹ and Valery I. Levitas^{2,3}

¹ *Department of Mechanical Engineering, Indian Institute of Technology Tirupati, Tirupati, A.P. 517506, India.*

² *Departments of Aerospace Engineering, Mechanical Engineering, and Material Science and Engineering, Iowa State University, Ames, IA 50011, USA.*

³ *Division of Materials Science and Engineering, Ames Laboratory, Ames, IA 50011, USA.*

A thermodynamically consistent multiphase phase-field approach for stress and temperature-induced martensitic phase transformation at the nanoscale and under large strains is developed. A total of N independent order parameters are considered for materials with N variants, where one of the order parameters describes $A \leftrightarrow M$ transformations and the remaining $N - 1$ independent order parameters describe the transformations between the variants. A non-contradictory gradient energy is used within the free energy of the system to account for the energies of the interfaces. In addition, a non-contradictory kinetic relationships for the rate of the order parameters versus thermodynamic driving forces is suggested. As a result, a system of consistent coupled Ginzburg-Landau equations for the order parameters are derived. The crystallographic solution for twins within twins is presented for the cubic to tetragonal transformations. A 3D complex twins within twins microstructure is simulated using the developed phase-field approach and a large-strain-based nonlinear finite element method. A comparative study between the crystallographic solution and the simulation result is presented.

Keywords: Multiphase phase-field approach; Martensitic transformations; Twins within twins; Crystallographic solution; Large strains; Finite element method.

1 Introduction

Martensitic transformations and microstructures. Martensitic transformations (MTs) are diffusionless solid-solid phase transformations observed in many metallic and nonmetallic crystalline solids, minerals, and various compounds, where a parent phase called austenite (high temperature phase) transforms into the product phase called martensite (low temperature phase) [1, 2]. The martensitic phase (here denoted by M) has lower crystallographic symmetry than the austenite phase (here denoted by A), and generally has multiple variants. Very complex microstructures such as austenite-twinned martensite,

twins within twins, twins within twins within twins, wedge, X-interfaces, etc., are observed within the materials undergoing MTs [1–5]. The evolution of such microstructures play a central role in, for example, strengthening of steel, shape memory effect in various alloys, ferromagnetic effect, caloric effects, etc [1, 6].

In continuum theories for MTs, such phase-changing materials are modeled as nonlinear elastic materials having multiple wells in the free energy density function [1, 2, 4, 7, 8]. Fine twinned microstructures associated with austenite-martensite interfaces, which were observed under the microscopes [9–12], are usually obtained as the minimizers of such non-convex energies within the continuum theories [4]. The analytical crystallographic solutions for twins between a pair of variants and the austenite-twinned martensite interfaces are well-known within the small as well as finite deformation theories [1, 2, 4, 13]. These solutions have been further used for more complex wedge microstructures [5, 14] and X-interfaces [15, 16]. Another important complex microstructure is twins within twins [1, 3] for which the general crystallographic equations were established in [1, 10, 11]. Though the governing equations are well-known for twins within twins, the analytical solutions to such microstructures are still missing to the best of our knowledge.

Phase-field approach to MTs. The phase-field approach based on the Ginzburg-Landau equations [17] (similar to Allen-Cahn’s approach [18]), which provides an ideal framework for studying the MTs, have been widely used for studying nucleation, growth of the phases, and evolution of complex microstructures [19–49]. A set of sufficiently smooth scalar internal variables called the order parameters, are used to describe the phases. The volume fraction based (e.g. [50–58]) or the transformation strains based (e.g. [19, 20, 23, 24, 26]) order parameters have been used. Important requirements for the interpolation functions are formulated in [45–48, 59]. Within the multiphase phase-field approaches, the order parameters should be constrained to some specified surfaces in order to control the transformation paths. To control the transformation paths, various constraint hypersurfaces such as hypersphere [60], planar surfaces [61], and straight lines [20, 62] have been used; see [20] for a review. The double-well [19, 20, 26, 60, 62] or double-obstacle [22] based thermal energies are usually used. The free energies are considered to be smooth functions of the order parameters, and the transformation strains are accepted as linear [50, 52–58] or nonlinear functions [19–21, 23, 24, 63] of the order parameters smoothly varying between all the phases, in particular, satisfying some additional requirements [45, 46]. First large-strain phase-field theory and computational approaches were presented in [21, 37, 47]. They utilized the methods of repetitive superposition of large strains, developed by Levin in [64–66] for viscoelastic materials, extended to materials with phase transformations.

A gradient (of the order parameters) based nonlocal energy is considered which introduces a finite interface width between the phases. The time evolution of these order parameters describing the kinetics of the PTs is derived using the laws of thermodynamics yielding a system of coupled Ginzburg-Landau equations. The interfacial stresses, consisting of the elastic and structural components and which play an important role in the nucleation of the phases and also in their kinetics and growth, have been considered [35, 67, 68]. A detailed comparison between these various multiphase phase-field approaches to MTs is presented in [20].

The multiphase phase-field model for studying the multivariant MTs developed by the authors in [20] yields non-contradictory results for a two-variant system. However, for a system with more than two variants, some contradictions have been observed in relation to the gradient energy and the system of kinetic equations. One of the aims of this work is to discuss those issues from that model and present a non-contradictory multiphase phase-field model for MTs. A gradient energy proposed therein simplifies consistently for a two-variant system and matches with the well-established result (see [20] for the discussion), but a contradiction is observed when the system contains more than two variants as discussed in Sec. 2.3. An alternative form of the gradient energy has been used here which has similarities with the gradient energy used in [22, 23, 53, 61] and yields non-contradictory results for any number of variants. In the present model, we however multiply this gradient term with the determinant of the total deformation gradient while determining the total system energy to ensure an appropriate form of the structural stress tensor, which was however not considered in [22, 23, 53, 61]. Furthermore, we point out in Sec. 2.5 that the coupled kinetic equations for the order parameters are non-contradictory for a two-variant system, but leads to contradictions for an N -variant system for $N > 2$, if the kinetic coefficients are assumed to be constants. We thus introduce a system of kinetic equations with kinetic coefficients which are step-wise functions of the order parameters and the driving forces, which is motivated from Ref. [55].

Contribution of the paper. The contributions of this paper are mainly two-fold:

i) We present a thermodynamically consistent nanoscale phase-field approach for multivariant MTs considering non-contradictory gradient energies and the local energies including the barrier, chemical, and elastic energy, as well as energies penalizing the multiphase junctions, while the deviations of the transformation paths for $A \leftrightarrow M$ and $M_i \leftrightarrow M_j$ PTs from the specified paths are appropriately controlled. The issues with the existing gradient energy models are discussed. Furthermore, a consistent kinetic model for coupled Ginzburg-Landau equations is derived, and the issues with the existing kinetic models are discussed. The present model can be used for MTs with any number of variants.

ii) The crystallographic solution for the twins within twins microstructure arising in cubic to tetragonal MTs are derived. The evolution and formation of 3D twins within twins microstructures in a single grain is studied using the present phase-field approach. The simulation results are in good agreement with the crystallographic solution and the experimental results.

Notations. The multiplication and the inner product between two arbitrary second order tensors \mathbf{A} and \mathbf{D} are denoted by $(\mathbf{A} \cdot \mathbf{D})_{ab} = A_{ac}D_{cb}$ and $\mathbf{A} : \mathbf{D} = A_{ab}D_{ba}$, respectively, where A_{ab} and D_{ab} are the components of the tensors in a right-handed orthonormal Cartesian basis $\{\mathbf{e}_1, \mathbf{e}_2, \mathbf{e}_3\}$. The repeated indices imply Einstein's summation. The Euclidean norm of \mathbf{A} is defined by $|\mathbf{A}| = \sqrt{\mathbf{A} : \mathbf{A}^T}$. The second-order identity tensor is denoted by \mathbf{I} . \mathbf{A}^T , $tr \mathbf{A}$, $det \mathbf{A}$, $sym(\mathbf{A})$, and $skew(\mathbf{A})$ denote the transpose, trace, determinant, symmetric part, and skew part of \mathbf{A} , respectively. For an invertible tensor \mathbf{A} , its inverse is denoted by \mathbf{A}^{-1} . The tensor or dyadic product between two arbitrary vectors \mathbf{a} and \mathbf{b} is denoted by $\mathbf{a} \otimes \mathbf{b}$. The reference, stress-free intermediate, and deformed or current configurations are denoted by Ω_0 , Ω_t , and Ω , respectively. The volumes in the reference and current configurations are denoted by V_0 and V , and their external boundaries are denoted by S_0 and S , respectively. The symbols $\nabla_0(\cdot)$ and $\nabla(\cdot)$ denote the gradient operators in Ω_0 and Ω , respectively. The Laplacian operators in Ω_0 and Ω are designated by $\nabla_0^2 := \nabla_0 \cdot \nabla_0$ and $\nabla^2 := \nabla \cdot \nabla$, respectively. The symbol $:=$ implies equality by definition.

2 Coupled mechanics and phase-field model

In this section, we describe our multiphase phase-field model, mostly based on [20] but with further development in terms of non-contradictory gradient energy and kinetic relationships between the rate of the order parameters and conjugated thermodynamical driving forces. The free energy used in the model is presented. The coupled elasticity equations and a new system of coupled Ginzburg-Landau equations are derived. A comparison of the present model with the previous models from the literature is also presented.

2.1 Order parameters

For the MTs in a system with austenite and N martensitic variants we consider $N + 1$ order parameters $\eta_0, \eta_1, \dots, \eta_i, \eta_j, \dots, \eta_N$, where η_0 describes $A \leftrightarrow M$ transformations such that $\eta_0 = 0$ in A and $\eta_0 = 1$ in M , and η_i (for $i = 1, \dots, N$) describes the variant M_i such that $\eta_i = 1$ in M_i and $\eta_i = 0$ in M_j for all $j \neq i$. Such descriptions for the order parameters were introduced by the authors in earlier work [20]. The order

parameters $\eta_1, \eta_2, \dots, \eta_N$ are constrained to lie on a plane by satisfying (see [20] for details)

$$\sum_{i=1}^N \eta_i = 1. \quad (2.1)$$

2.2 Kinematics

The position vector of a particle in the deformed configuration Ω at time instance t is given by $\mathbf{r}(\mathbf{r}_0, t) = \mathbf{r}_0 + \mathbf{u}(\mathbf{r}_0, t)$, where \mathbf{r}_0 is the position vector of that particle in Ω_0 , and \mathbf{u} is the displacement vector. We consider the following multiplicative decomposition for the total deformation gradient \mathbf{F} [67]:

$$\mathbf{F} := \nabla_0 \mathbf{r} = \mathbf{F}_e \cdot \mathbf{F}_t = \mathbf{V}_e \cdot \mathbf{R} \cdot \mathbf{U}_t, \quad (2.2)$$

where the subscripts e and t denote elastic and transformational parts, respectively, and \mathbf{F}_e and \mathbf{F}_t are the elastic and transformational parts of \mathbf{F} . The tensors \mathbf{F}_e and \mathbf{F}_t are also decomposed into $\mathbf{F}_e = \mathbf{V}_e \cdot \mathbf{R}_e$ and $\mathbf{F}_t = \mathbf{R}_t \cdot \mathbf{U}_t$, respectively, where \mathbf{V}_e is the left elastic stretch tensor (symmetric), \mathbf{U}_t is the right transformation stretch tensor (symmetric), and \mathbf{R}_e and \mathbf{R}_t are rotations. In Eq. (2.2) we have used $\mathbf{R} = \mathbf{R}_e \cdot \mathbf{R}_t$. We denote $J = \det \mathbf{F}$, $J_t = \det \mathbf{F}_t$, and $J_e = \det \mathbf{F}_e$. Hence, by Eq. (2.2), $J = J_t J_e$. The Lagrangian total and elastic strain tensors are defined as

$$\mathbf{E} := 0.5(\mathbf{C} - \mathbf{I}), \quad \text{and} \quad \mathbf{E}_e := 0.5(\mathbf{C}_e - \mathbf{I}), \quad (2.3)$$

respectively, where $\mathbf{C} = \mathbf{F}^T \cdot \mathbf{F}$, and $\mathbf{C}_e = \mathbf{F}_e^T \cdot \mathbf{F}_e$. We define another measure of the total and elastic strain tensors as

$$\mathbf{b} = 0.5(\mathbf{B} - \mathbf{I}), \quad \text{and} \quad \mathbf{b}_e = 0.5(\mathbf{B}_e - \mathbf{I}), \quad (2.4)$$

respectively, where $\mathbf{B} = \mathbf{F} \cdot \mathbf{F}^T = \mathbf{V}^2$, $\mathbf{B}_e = \mathbf{F}_e \cdot \mathbf{F}_e^T = \mathbf{V}_e^2$, and $\mathbf{V} = \sqrt{\mathbf{B}}$ is the left total stretch tensor. *Kinematic model for \mathbf{F}_t .* We consider \mathbf{F}_t as a linear combination of the Bain strains multiplied by the interpolation functions related to the order parameters [20]:

$$\mathbf{F}_t = \mathbf{U}_t = \mathbf{I} + \sum_{i=1}^N (\mathbf{U}_{ti} - \mathbf{I}) \varphi(a_\varepsilon, \eta_0) \phi_i(\eta_i), \quad (2.5)$$

where \mathbf{U}_{ti} is the Bain stretch tensor for \mathbf{M}_i . We take the interpolation functions $\varphi(a_\varepsilon, \eta_0)$ and $\phi_i(\eta_i)$ as [20]

$$\begin{aligned} \varphi(a_\varepsilon, \eta_0) &= a_\varepsilon \eta_0^2 + (4 - 2a_\varepsilon) \eta_0^3 + (a_\varepsilon - 3) \eta_0^4, \quad \text{and} \\ \phi_i(\eta_i) &= \eta_i^2 (3 - 2\eta_i) \quad \text{for all } i = 1, 2, \dots, N, \end{aligned} \quad (2.6)$$

respectively, which satisfy the following conditions derived from the requirement of thermodynamic equilibrium of the homogeneous phases:

$$\begin{aligned} \varphi(a_\varepsilon, 0) = 0, \quad \varphi(a_\varepsilon, 1) = 1, \quad \text{and} \quad \frac{\partial \varphi(a_\varepsilon, 0)}{\partial \eta_0} = \frac{\partial \varphi(a_\varepsilon, 1)}{\partial \eta_0} = 0; \\ \phi_i(0) = 0, \quad \phi_i(1) = 1, \quad \text{and} \quad \frac{\partial \phi_i(\eta_i = 0)}{\partial \eta_i} = \frac{\partial \phi_i(\eta_i = 1)}{\partial \eta_i} = 0 \quad \text{for all } i = 1, 2, \dots, N. \end{aligned} \quad (2.7)$$

The constant a_ε in Eq. (2.6) must be within the range $0 \leq a_\varepsilon \leq 6$ [67].

2.3 Free energy

We assume the Helmholtz free energy per unit mass of the body as [20, 67]:

$$\psi(\mathbf{F}, \theta, \eta_0, \eta_i, \nabla \eta_0, \nabla \eta_i) = \psi^l(\mathbf{F}_e, \theta, \eta_0, \eta_i) + J\psi^\nabla(\eta_0, \nabla \eta_0, \nabla \eta_i), \quad (2.8)$$

where $\psi^l(\mathbf{F}_e, \theta, \eta_0, \eta_i)$ is the local part of the free energy density and $\psi^\nabla(\eta_0, \nabla \eta_0, \nabla \eta_i)$ is the gradient based nonlocal energy accounting for the energies of all the interfaces. We have taken ψ^l as

$$\psi^l(\mathbf{F}_e, \theta, \eta_0, \eta_i) = \frac{J_t}{\rho_0} \psi_e(\mathbf{F}_e, \theta, \eta_0, \eta_i) + J\check{\psi}^\theta(\theta, \eta_0, \eta_i) + \tilde{\psi}^\theta(\theta, \eta_0, \eta_i) + \psi_p(\eta_0, \eta_i), \quad (2.9)$$

where ψ_e is the strain energy per unit volume in Ω_t , $\check{\psi}^\theta$ is the barrier energy related to $\mathbf{A} \leftrightarrow \mathbf{M}$ PT and all the variant \leftrightarrow variant transformations, $\tilde{\psi}^\theta$ is the thermal/chemical energy for $\mathbf{A} \leftrightarrow \mathbf{M}$ transformations, ψ_p penalizes various triple and higher junctions between all the phases and also accounts for the penalization in energies for the deviation of the transformation paths from the assigned ones, $\theta > 0$ is the absolute temperature, and ρ_0 is the density of the solid in Ω_0 . In Eqs. (2.8) and (2.9), the barrier energy and the gradient energy are multiplied by J following [67] in order to obtain the desired expression for the structural stresses; see Eq. (2.29). Any material property B for each particle of the body are determined using [20]

$$B(\eta_0, \eta_i, \theta, \mathbf{F}) = B_0(1 - \varphi(a, \eta_0)) + \varphi(a, \eta_0) \sum_{i=1}^N B_i \phi_i(\eta_i), \quad (2.10)$$

where B_0 and B_i are the material properties of the homogeneous phases \mathbf{A} and \mathbf{M}_i , respectively, $\varphi(a, \eta_0)$ has the same expression as $\varphi(a_\varepsilon, \eta_0)$ given by Eq. (2.6)₁ when a_ε is replaced by a therein.

The expressions for all the energies introduced in Eqs. (2.8) and (2.9) are given below:

(i) *Strain energy*: We consider ψ_e as [20]

$$\psi_e = 0.5 \mathbf{E}_e : \hat{\mathcal{C}}_e(\eta_0, \eta_i) : \mathbf{E}_e, \quad (2.11)$$

where the fourth-order elastic modulus tensor at any particle is taken following Eq. (2.10) as [20]

$$\hat{\mathcal{C}}_e(\eta_0, \eta_i) = (1 - \varphi(a, \eta_0))\hat{\mathcal{C}}_{(e)0} + \varphi(a, \eta_0) \sum_{i=1}^N \phi_i(\eta_i)\hat{\mathcal{C}}_{(e)i}, \quad (2.12)$$

and $\hat{\mathcal{C}}_{(e)0}$ and $\hat{\mathcal{C}}_{(e)i}$ are the fourth order elastic modulus tensors of A and M_i , respectively.

(ii) *Barrier energy*: The total energy of the barriers between A and M and between all the variants is [20]

$$\psi^\theta = A_{0M} \eta_0^2 (1 - \eta_0)^2 + \varphi(a_b, \eta_0) \tilde{A} \sum_{i=1}^{N-1} \sum_{j=i+1}^N \eta_i^2 \eta_j^2, \quad (2.13)$$

where A_{0M} and \tilde{A} are the coefficients for the barrier energies between A and M, and M_i and M_j (for all $i \neq j$), respectively.

(iii) *Thermal energy*: The thermal energy of a particle undergoing A \leftrightarrow M PTs is taken as [20, 45–47]

$$\tilde{\psi}^\theta = \psi_0^\theta(\theta) + \eta_0^2 (3 - 2\eta_0) \Delta\psi^\theta(\theta), \quad \text{where } \Delta\psi^\theta = -\Delta s_{0M}(\theta - \theta_e), \quad (2.14)$$

ψ_0^θ is the thermal energy of A, $\Delta\psi^\theta = \psi_M^\theta - \psi_0^\theta$ is the thermal energy difference between A and M phases, $\Delta s_{0M} = s_M - s_0$, s_0 and s_M are the entropies of A and M, respectively, per unit volume, and θ_e is the thermodynamic equilibrium temperature between A and M phases.

(iv) *Gradient energy*: We consider the gradient energy, taking all the interfacial energies into consideration, as

$$\psi^\nabla = \frac{\beta_{0M}}{2\rho_0} |\nabla\eta_0|^2 + \frac{1}{2\rho_0} \tilde{\varphi}(\eta_0, a_\beta, a_c) \sum_{i=1}^{N-1} \sum_{j=i+1}^N \beta_{ij} \nabla\eta_i \cdot \nabla\eta_j, \quad (2.15)$$

where the interpolation function $\tilde{\varphi}$ is taken as [20]

$$\tilde{\varphi}(a_\beta, a_c, \eta_0) = a_c + a_\beta \eta_0^2 - 2[a_\beta - 2(1 - a_c)]\eta_0^3 + [a_\beta - 3(1 - a_c)]\eta_0^4, \quad (2.16)$$

where the constant is taken as $0 < a_c \ll 1$, and the purpose of considering it in Eq. (2.16) is discussed in [20]. In Eq. (2.15), β_{0M} and β_{ij} are the gradient energy coefficients for A-M and M_i - M_j interfaces, respectively. In Eq. (2.16) a_β and a_c are constant parameters. The gradient energy similar to Eq. (2.15) was earlier used in [53, 61]. Notably, the authors earlier introduced another form of the gradient energy in [20] given by

$$\psi^\nabla = \frac{1}{2\rho_0} \left[\beta_{0M} |\nabla\eta_0|^2 + \sum_{i=1}^N \sum_{j=1, \neq i}^N \frac{\beta_{ij}}{8} |\nabla\eta_i - \nabla\eta_j|^2 \tilde{\varphi}(\eta_0, a_\beta, a_0) \right]. \quad (2.17)$$

This energy given by Eq. (2.17) simplifies to

$$\psi^\nabla = \frac{1}{2\rho_0}\beta_{0M}|\nabla\eta_0|^2 + \frac{\tilde{\varphi}(\eta_0, a_\beta, a_0)}{8\rho_0} \left(\beta_{12}|\nabla\eta_1 - \nabla\eta_2|^2 + \beta_{21}|\nabla\eta_2 - \nabla\eta_1|^2 \right), \quad (2.18)$$

for a system with two variants, where applying the constraint $\eta_1 + \eta_2 = 1$ and $\beta_{12} = \beta_{21}$ due to the symmetry [67] we further simplify it to

$$\psi^\nabla = \frac{1}{2\rho_0}\beta_{0M}|\nabla\eta_0|^2 + \frac{\tilde{\varphi}(\eta_0, a_\beta, a_0)}{2\rho_0}\beta_{12}|\nabla\eta_1|^2, \quad (2.19)$$

which is consistent with the results of earlier models; see e.g. [67] and the references therein. We would like to mention that the coefficients β_{ij} in Eq. (2.17) for the variant pairs which are in twin relationships would be much smaller than that for the variant pairs which are not in twin relationships. For a system with three variants, Eq. (2.17) reduces to

$$\begin{aligned} \psi^\nabla = & \frac{\beta_{0M}}{2\rho_0}|\nabla\eta_0|^2 + \frac{1}{8\rho_0} \left[(\beta_{12} + \beta_{13})|\nabla\eta_1|^2 + (\beta_{12} + \beta_{23})|\nabla\eta_2|^2 + (\beta_{13} + \beta_{23})|\nabla\eta_3|^2 - \right. \\ & \left. 2(\beta_{12}\nabla\eta_1 \cdot \nabla\eta_2 + \beta_{23}\nabla\eta_2 \cdot \nabla\eta_3 + \beta_{13}\nabla\eta_1 \cdot \nabla\eta_3) \right] \tilde{\varphi}(\eta_0, a_\beta, a_0). \end{aligned} \quad (2.20)$$

Let us consider a region for such a three-variant system where only M_1 and M_2 coexist and M_3 is absent, i.e. $\eta_3 = 0$ and $\eta_1 + \eta_2 = 1$. The gradient energy given by Eq. (2.20) in that region is rewritten by applying these conditions as

$$\psi^\nabla = \frac{\beta_{0M}}{2\rho_0}|\nabla\eta_0|^2 + \frac{1}{8\rho_0}(\beta_{23} + \beta_{13} + 4\beta_{12})|\nabla\eta_1|^2 \tilde{\varphi}(\eta_0, a_\beta, a_0). \quad (2.21)$$

Obviously, the energy parameters β_{23} and β_{13} are going to influence the interfacial energy M_1 and M_2 variants, which is nonphysical; see also [69] for an analysis. We have shown that the gradient energy given by Eq. (2.17) yields a nonphysical contribution for an interface between two variants from the gradient coefficients which are not related to that interface, and hence this form of gradient energy is not acceptable. However, the energy given by Eq. (2.15) is non-contradictory for any number of variants, and hence it is accepted in this paper.

(v) *Penalization energy for junctions*: We penalize the triple and higher junctions between all the phases and the deviations of the transformation paths between the variants using [20]

$$\begin{aligned} \psi_p = & \sum_{i=1}^{N-1} \sum_{j=i+1}^N K_{ij}(\eta_i + \eta_j - 1)^2 \eta_i^2 \eta_j^2 + [1 - \varphi(a_K, \eta_0)] \sum_{i=1}^{N-1} \sum_{j=i+1}^N K_{0ij} \eta_0^2 \eta_i^2 \eta_j^2 + \sum_{i=1}^{N-2} \sum_{j=i+1}^{N-1} \sum_{k=j+1}^N K_{ijk} \eta_i^2 \eta_j^2 \eta_k^2 + \\ & [1 - \varphi(a_K, \eta_0)] \sum_{i=1}^{N-2} \sum_{j=i+1}^{N-1} \sum_{k=j+1}^N K_{0ijk} \eta_0^2 \eta_i^2 \eta_j^2 \eta_k^2 + \sum_{i=1}^{N-3} \sum_{j=i+1}^{N-2} \sum_{k=j+1}^{N-1} \sum_{l=k+1}^N K_{ijkl} \eta_i^2 \eta_j^2 \eta_k^2 \eta_l^2, \quad \text{where} \\ K_{ii} = & K_{0ii} = K_{iji} = K_{iik} = K_{0iji} = K_{0iik} = K_{ijil} = K_{iikl} = K_{ijjl} = K_{ijkk} = 0. \end{aligned} \quad (2.22)$$

In Eq. (2.22), the parameter $K_{ij} \geq 0$ controls the penalization of the deviation of the $M_j \leftrightarrow M_i$ transformation path from the straight line $\eta_j + \eta_i = 1$ for all $\eta_k = 0$ and $k \neq j, i$; the constant coefficients $K_{0ij} \geq 0$, $K_{ijk} \geq 0$, $K_{0ijk} \geq 0$, and $K_{ijkl} \geq 0$ are related to the penalization of the junctions between A- M_i - M_j , M_i - M_j - M_k , A- M_i - M_j - M_k , and M_i - M_j - M_k - M_l , respectively.

In the absence of all the penalty terms, i.e. when $K_{ij} = K_{0ij} = K_{0ik} = K_{0jk} = K_{ijk} = K_{0ijk} = 0$, we can show that for a martensitic region ($\eta_0 = 1$) with three variants, say, M_1 , M_2 and M_3 , the barrier energy (see Eq. (2.13)) in the middle of the triple junction region, i.e., at the point with $\eta_1 = \eta_2 = \eta_3 = 1/3$ is $3 \times \bar{A}/81 = \bar{A}/27$ which is less than the barrier energy $\bar{A}/16$ at the middle line of any variant-variant interface (a line with, say, $\eta_1 = \eta_2 = 1/2$ and $\eta_3 = 0$). Hence when $K_{123} \neq 0$ the total energy at a martensitic particle with $\eta_1 = \eta_2 = \eta_3 = 1/3$ is

$$E_{TJ}|_{\eta_1=\eta_2=\eta_3=1/3} = \frac{\bar{A}}{27} + \frac{K_{123}}{729}. \quad (2.23)$$

It is to be noted that Tóth et al. [70] and Bollada et al. [69] considered barrier energy similar to ours given by Eq. (2.13) but with a common multiplication factor to incorporate higher energy at the junction region as compared to the respective interface regions. In this paper, we have, however, followed a different and simpler approach for that purpose, where we have introduced the penalty terms in the free energy, and by varying the coefficients K_{0ij} , K_{0ik} , K_{0jk} , K_{ijk} , K_{0ijk} we can control the energy of all the junction regions. For example, by tuning the parameter K_{123} in Eq. (2.23), we can make the barrier energy height at the junction region higher than the barrier energy in the interfacial region. A quantitative comparison between our formulation and the approach in [69, 70] is however not given here.

2.4 Governing equations

We now present the governing equations. Applying the principle of balance of linear and angular momentum, and the first and second law of thermodynamics, and using an approach similar to [20, 67], we derive the mechanical equilibrium equation, and the dissipation inequalities listed below.

2.4.1 Mechanical equilibrium equations and stresses

The mechanical equilibrium equation is given by [20, 67]

$$\nabla_0 \cdot \mathbf{P} = \mathbf{0} \quad \text{in } \Omega_0, \quad \text{or} \quad \nabla \cdot \boldsymbol{\sigma} = \mathbf{0} \quad \text{in } \Omega, \quad (2.24)$$

where the body forces and inertia are neglected, \mathbf{P} is the total first Piola-Kirchhoff stress tensor, and $\boldsymbol{\sigma}$ is the total Cauchy stress tensor which is symmetric. The total stresses are composed of their respective

elastic and structural parts [20]:

$$\mathbf{P} = \mathbf{P}_e + \mathbf{P}_{st}, \quad \text{and} \quad \boldsymbol{\sigma} = \boldsymbol{\sigma}_e + \boldsymbol{\sigma}_{st}. \quad (2.25)$$

The elastic stresses are given by [20, 67]

$$\mathbf{P}_e = J_t \mathbf{F}_e \cdot \hat{\mathbf{S}}_e \cdot \mathbf{F}_t^{-T}, \quad \text{and} \quad \boldsymbol{\sigma}_e = J_e^{-1} \mathbf{F}_e \cdot \hat{\mathbf{S}}_e \cdot \mathbf{F}_e^T, \quad (2.26)$$

where $\hat{\mathbf{S}}_e = \frac{\partial \psi_e(\mathbf{E}_e)}{\partial \mathbf{E}_e}$. For an isotropic elastic response, \mathbf{P}_e and $\boldsymbol{\sigma}_e$ can alternatively be expressed as

$$\mathbf{P}_e = J_t \mathbf{V}_e^2 \cdot \frac{\partial \psi_e(\mathbf{b}_e)}{\partial \mathbf{b}_e} \cdot \mathbf{F}^{-T}, \quad \text{and} \quad \boldsymbol{\sigma}_e = J_e^{-1} \mathbf{V}_e^2 \cdot \frac{\partial \psi_e(\mathbf{b}_e)}{\partial \mathbf{b}_e}, \quad (2.27)$$

respectively. The general forms of structural stress tensors are given by [20, 67]

$$\begin{aligned} \mathbf{P}_{st} &= J\rho_0(\check{\psi}^\theta + \psi^\nabla) \mathbf{F}^{-T} - J\rho_0 \left(\nabla\eta_0 \otimes \frac{\partial \psi^\nabla}{\partial \nabla\eta_0} + \sum_{i=1}^N \nabla\eta_i \otimes \frac{\partial \psi^\nabla}{\partial \nabla\eta_i} \right) \cdot \mathbf{F}^{-T}, \quad \text{and} \\ \boldsymbol{\sigma}_{st} &= \rho_0(\check{\psi}^\theta + \psi^\nabla) \mathbf{I} - \rho_0 \left(\nabla\eta_0 \otimes \frac{\partial \psi^\nabla}{\partial \nabla\eta_0} + \sum_{i=1}^N \nabla\eta_i \otimes \frac{\partial \psi^\nabla}{\partial \nabla\eta_i} \right). \end{aligned} \quad (2.28)$$

Using the gradient energy given by Eq. (2.15) in Eq. (2.28)_{1,2}, the exact form of the structural stresses are obtained as

$$\begin{aligned} \mathbf{P}_{st} &= J\rho_0(\check{\psi}^\theta + \psi^\nabla) \mathbf{F}^{-T} - J\beta_{0M} \nabla\eta_0 \otimes \nabla\eta_0 \cdot \mathbf{F}^{-T} - J\tilde{\varphi} \left(\sum_{i=1}^{N-1} \sum_{j=i+1}^N \beta_{ij} \nabla\eta_i \otimes \nabla\eta_j \right) \cdot \mathbf{F}^{-T}, \quad \text{and} \\ \boldsymbol{\sigma}_{st} &= \rho_0(\check{\psi}^\theta + \psi^\nabla) \mathbf{I} - \beta_{0M} \nabla\eta_0 \otimes \nabla\eta_0 - \tilde{\varphi} \left(\sum_{i=1}^{N-1} \sum_{j=i+1}^N \beta_{ij} \nabla\eta_i \otimes \nabla\eta_j \right). \end{aligned} \quad (2.29)$$

2.5 Dissipation inequality and Ginzburg-Landau equations

The dissipation inequalities for the order parameter η_0 and also for the order parameter η_1, \dots, η_N are obtained as (see [20] for the details)

$$D_0 = \dot{\eta}_0 X_0 \geq 0 \quad \text{and} \quad D_M = \sum_{i=1}^N \dot{\eta}_i X_i \geq 0, \quad (2.30)$$

respectively, where the conjugate ‘forces’ X_0 and X_i correspond to the ‘fluxes’ $\dot{\eta}_0$ and $\dot{\eta}_i$, respectively, are given by

$$X_k = -\rho_0 \frac{\partial \psi}{\partial \eta_k} + \nabla_0 \cdot \left(\rho_0 J \frac{\partial \psi^\nabla}{\partial \nabla_0 \eta_k} \right) \quad \text{for all } k = 0, 1, \dots, N. \quad (2.31)$$

Using Eqs. (2.8) and (2.9) in (2.31) and also applying the following identities (for all $k = 0, 1, \dots, N$)

$$\nabla_0 \eta_k = \mathbf{F}^t \cdot \nabla \eta_k, \quad (2.32)$$

$$\frac{\partial \psi^\nabla}{\partial \nabla_0 \eta_k} = \mathbf{F}^{-1} \cdot \frac{\partial \psi^\nabla}{\partial \nabla \eta_k}, \quad (2.33)$$

which can be easily proved using the indicial notations, we get the conjugate forces X_0 and X_i (for all $i = 1, \dots, N$) as

$$\begin{aligned} X_0 = & (\mathbf{P}_e^T \cdot \mathbf{F} - J_t \psi_e \mathbf{I}) : \mathbf{F}_t^{-1} \cdot \frac{\partial \mathbf{F}_t}{\partial \eta_0} - J_t \left. \frac{\partial \psi_e}{\partial \eta_0} \right|_{\mathbf{F}_e} - \rho_0 (6\eta_0 - 6\eta_0^2) \Delta \psi^\theta - J \rho_0 \tilde{A} \sum_{i=1}^{N-1} \sum_{j=i+1}^N \eta_i^2 \eta_j^2 \frac{\partial \varphi(a_b, \eta_0)}{\partial \eta_0} - \\ & J \rho_0 [A_{0M}(\theta) + (a_\theta - 3) \Delta \psi^\theta(\theta)] (2\eta_0 - 6\eta_0^2 + 4\eta_0^3) - \frac{J}{2} \frac{\partial \tilde{\varphi}(a_\beta, a_c, \eta_0)}{\partial \eta_0} \sum_{i=1}^{N-1} \sum_{j=i+1}^N \beta_{ij} (\mathbf{C}^{-1} \cdot \nabla_0 \eta_i) \cdot \nabla_0 \eta_j - \\ & \rho_0 \left(\sum_{i=1}^{N-1} \sum_{j=i+1}^N K_{0ij} \eta_i^2 \eta_j^2 + \sum_{i=1}^{N-2} \sum_{j=i+1}^{N-1} \sum_{k=j+1}^N K_{0ijk} \eta_i^2 \eta_j^2 \eta_k^2 \right) \left[2(1 - \varphi(a_K, \eta_0)) \eta_0 - \frac{\partial \varphi(a_K, \eta_0)}{\partial \eta_0} \eta_0^2 \right] + \\ & \nabla_0 \cdot (J \beta_{0M} \nabla_0 \eta_0); \end{aligned} \quad (2.34)$$

$$\begin{aligned} X_i = & (\mathbf{P}_e^T \cdot \mathbf{F} - J_t \psi_e \mathbf{I}) : \mathbf{F}_t^{-1} \cdot \frac{\partial \mathbf{F}_t}{\partial \eta_i} - J_t \left. \frac{\partial \psi_e}{\partial \eta_i} \right|_{\mathbf{F}_e} - 2J \rho_0 \tilde{A} \sum_{j=1, \neq i}^N \eta_i \eta_j^2 \varphi(a_b, \eta_0) - 2\rho_0 \sum_{j=1}^N K_{ij} (\eta_i + \eta_j - 1) \times \\ & (2\eta_i + \eta_j - 1) \eta_j^2 \eta_i - 2\rho_0 \left(\sum_{j=1}^N K_{0ij} \eta_j^2 + \sum_{j=1}^{N-1} \sum_{k=j+1}^N K_{0ijk} \eta_j^2 \eta_k^2 \right) \eta_0^2 \eta_i (1 - \varphi(a_K, \eta_0)) - \\ & 2\rho_0 \sum_{j=1}^{N-1} \sum_{k=j+1}^N K_{ijk} \eta_i \eta_j^2 \eta_k^2 - 2\rho_0 \sum_{j=1}^{N-2} \sum_{k=j+1}^{N-1} \sum_{l=k+1}^N K_{ijkl} \eta_i \eta_j^2 \eta_k^2 \eta_l^2 + \\ & \nabla_0 \cdot \left(\tilde{\varphi}(a_\beta, a_c, \eta_0) J \sum_{j=1}^N \beta_{ij} \nabla_0 \eta_j \right) \quad \text{for all } i = 1, 2, 3, \dots, N. \end{aligned} \quad (2.35)$$

In Eqs. (2.34) and (2.35) the conjugate forces are expressed with respect to the field variables in the reference configuration Ω_0 .

Alternatively, these forces can be expressed with respect to the field variables in Ω as follows. Using the following identity (see e.g. Chapter 2 of [71])

$$\nabla_0 \cdot (\text{Cof } \mathbf{F}) = \nabla_0 \cdot (J \mathbf{F}^{-t}) = \mathbf{0}, \quad (2.36)$$

we can rewrite the conjugate force X_l given by Eq. (2.31) in terms of the derivative with respect to $\Omega(t)$ as

$$X_k = -J \rho \frac{\partial \psi}{\partial \eta_k} + J \nabla \cdot \left(\rho_0 \frac{\partial \psi^\nabla}{\partial \nabla \eta_k} \right) = J \left[-\frac{\partial(\rho \psi)}{\partial \eta_k} + \nabla \cdot \left(\frac{\partial(\rho J \psi^\nabla)}{\partial \nabla \eta_k} \right) \right] \quad \text{for all } k = 0, 1, \dots, N. \quad (2.37)$$

The conjugate forces given by Eqs. (2.34) and (2.35) can be rewritten in terms of the Cauchy stress and

the gradient operator $\nabla(\cdot)$ as

$$\begin{aligned}
X_0 = & \left(J\mathbf{F}^{-1} \cdot \boldsymbol{\sigma}_e \cdot \mathbf{F} - J_t \psi_e \mathbf{I} \right) : \mathbf{F}_t^{-1} \cdot \frac{\partial \mathbf{F}_t}{\partial \eta_0} - J_t \left. \frac{\partial \psi_e}{\partial \eta_0} \right|_{\mathbf{F}_e} - \rho_0 (6\eta_0 - 6\eta_0^2) \Delta \psi^\theta - J\rho_0 \tilde{A} \sum_{i=1}^{N-1} \sum_{j=i+1}^N \eta_i^2 \eta_j^2 \frac{\partial \varphi(a_b, \eta_0)}{\partial \eta_0} - \\
& J\rho_0 [A_{0M}(\theta) + (a_\theta - 3) \Delta \psi^\theta(\theta)] (2\eta_0 - 6\eta_0^2 + 4\eta_0^3) - \frac{J}{2} \frac{\partial \tilde{\varphi}(a_\beta, a_c, \eta_0)}{\partial \eta_0} \sum_{i=1}^{N-1} \sum_{j=i+1}^N \beta_{ij} \nabla \eta_i \cdot \nabla \eta_j - \\
& \rho_0 \left(\sum_{i=1}^{N-1} \sum_{j=i+1}^N K_{0ij} \eta_i^2 \eta_j^2 + \sum_{i=1}^{N-2} \sum_{j=i+1}^{N-1} \sum_{k=j+1}^N K_{0ijk} \eta_i^2 \eta_j^2 \eta_k^2 \right) \left[2(1 - \varphi(a_K, \eta_0)) \eta_0 - \frac{\partial \varphi(a_K, \eta_0)}{\partial \eta_0} \eta_0^2 \right] + \\
& J\nabla \cdot (\beta_{0M} \nabla \eta_0); \tag{2.38}
\end{aligned}$$

$$\begin{aligned}
X_i = & \left(J\mathbf{F}^{-1} \cdot \boldsymbol{\sigma}_e \cdot \mathbf{F} - J_t \psi_e \mathbf{I} \right) : \mathbf{F}_t^{-1} \cdot \frac{\partial \mathbf{F}_t}{\partial \eta_i} - J_t \left. \frac{\partial \psi_e}{\partial \eta_i} \right|_{\mathbf{F}_e} - 2J\rho_0 \tilde{A} \sum_{j=1, \neq i}^N \eta_i \eta_j^2 \varphi(a_b, \eta_0) - 2\rho_0 \sum_{j=1}^N K_{ij} (\eta_i + \eta_j - 1) \times \\
& (2\eta_i + \eta_j - 1) \eta_j^2 \eta_i - 2\rho_0 \left(\sum_{j=1}^N K_{0ij} \eta_j^2 + \sum_{j=1}^{N-1} \sum_{k=j+1}^N K_{0ijk} \eta_j^2 \eta_k^2 \right) \eta_0^2 \eta_i (1 - \varphi(a_K, \eta_0)) - \\
& 2\rho_0 \sum_{j=1}^{N-1} \sum_{k=j+1}^N K_{ijk} \eta_i \eta_j^2 \eta_k^2 - 2\rho_0 \sum_{j=1}^{N-2} \sum_{k=j+1}^{N-1} \sum_{l=k+1}^N K_{ijkl} \eta_i \eta_j^2 \eta_k^2 \eta_l^2 + \\
& J\nabla \cdot \left(\tilde{\varphi}(a_\beta, a_c, \eta_0) \sum_{j=1}^N \beta_{ij} \nabla \eta_j \right) \quad \text{for all } i = 1, 2, 3, \dots, N. \tag{2.39}
\end{aligned}$$

From the dissipation inequality (2.30)₁ we derive the kinetic law for η_0 as

$$\dot{\eta}_0 = L_{0M} X_0, \tag{2.40}$$

where $L_{0M} > 0$ is the kinetic coefficient for $\mathbf{A} \leftrightarrow \mathbf{M}$ PTs. In order to derive the kinetic laws for the order parameters η_1, \dots, η_N using the inequality (2.30)₂, we introduce

$$\dot{\eta}_i = \sum_{j=1}^N \dot{\eta}_{ij}, \quad \text{where } \dot{\eta}_{ij} = -\dot{\eta}_{ji} \text{ and } \dot{\eta}_{ii} = 0 \quad \text{for all } i, j = 1, \dots, N. \tag{2.41}$$

Using Eq. (2.41), the dissipation rate due to the evolution of the martensitic variants given by Eq. (2.30)₂

is rewritten as

$$\begin{aligned}
D_M &= \sum_{i=1}^N \dot{\eta}_i X_i = \sum_{i=1}^N \sum_{j=1}^N X_i \dot{\eta}_{ij} \quad (\text{using Eq. (2.41)}_1) \\
&= \sum_{i=1}^N \sum_{j=1}^N X_{ij} \dot{\eta}_{ij} + \sum_{i=1}^N \sum_{j=1}^N X_j \dot{\eta}_{ij} \quad (\text{using } X_{ij} = X_i - X_j) \\
&= \sum_{i=1}^N \sum_{j=1}^N X_{ij} \dot{\eta}_{ij} - \sum_{i=1}^N \sum_{j=1}^N X_j \dot{\eta}_{ji} \quad (\text{using Eq. (2.41)}_2) \\
&= \sum_{i=1}^N \sum_{j=1}^N X_{ij} \dot{\eta}_{ij} - \sum_{i=1}^N \sum_{j=1}^N X_i \dot{\eta}_{ij} \quad (\text{swapping the indices in the second term}) \\
&= \sum_{i=1}^N \sum_{j=1}^N X_{ij} \dot{\eta}_{ij} - \sum_{i=1}^N X_i \dot{\eta}_i. \tag{2.42}
\end{aligned}$$

Noticing that the second term on the right-hand side of Eq. (2.42) is equal to D_M (compare with Eq. (2.30)₂) we obtain

$$D_M = \frac{1}{2} \sum_{i=1}^N \sum_{j=1}^N X_{ij} \dot{\eta}_{ij} = \sum_{j=1}^{N-1} \sum_{i=j+1}^N X_{ij} \dot{\eta}_{ij} \geq 0. \tag{2.43}$$

Using the inequality (2.43) we derive the Ginzburg-Landau equations for the evolution of the variants as

$$\dot{\eta}_{ij} = L_{ij}(X_i - X_j), \tag{2.44}$$

where $L_{ij} \geq 0$ is the kinetic coefficient for transformations between M_i and M_j and is taken as in [55]

$$L_{ij} \begin{cases} \neq 0 & \text{if } (X_i - X_j) \geq 0 \quad \text{and} \quad \{0 \leq \eta_i < 1 \ \& \ 0 < \eta_j \leq 1\} \\ \neq 0 & \text{if } (X_i - X_j) \leq 0 \quad \text{and} \quad \{0 < \eta_i \leq 1 \ \& \ 0 \leq \eta_j < 1\} \\ = 0 & \text{if } (X_i - X_j) \geq 0 \quad \text{and} \quad \{\eta_i = 1 \text{ or } \eta_j = 0\} \\ = 0 & \text{if } (X_i - X_j) \leq 0 \quad \text{and} \quad \{\eta_i = 0 \text{ or } \eta_j = 1\}. \end{cases} \tag{2.45}$$

Substituting Eq. (2.44) in Eq. (2.41) the Ginzburg-Landau equations for all N order parameters η_1, \dots, η_N are obtained as

$$\dot{\eta}_i = \sum_{j=1, j \neq i}^N L_{ij}(X_i - X_j). \tag{2.46}$$

We note that L_{ij} in Eq. (2.46) and defined in Eq. (2.45) are piece-wise constant, jumping between their finite values and zero depending on the driving forces and the order parameters. If L_{ij} is simply assumed to be constants similar to our earlier work in [20], an issue would arise. To understand it clearly, let us consider, without any loss of generality, a three-variant martensitic system (where $\eta_0 = 1$) with M_1 , M_2 , and M_3 . Using the constraint $\eta_1 + \eta_2 + \eta_3 = 1$, the two independent Ginzburg-Landau equations from

Eq. (2.46), when expressed for $\dot{\eta}_1$ and $\dot{\eta}_2$, are given by

$$\dot{\eta}_1 = L_{12}(X_1 - X_2) + L_{13}(X_1 - X_3) \quad \text{and} \quad \dot{\eta}_2 = L_{12}(X_2 - X_1) + L_{23}(X_2 - X_3). \quad (2.47)$$

We now consider a martensitic region in the domain where M_3 is absent and only the variants M_1 and M_2 are evolving within an arbitrary time interval. The order parameters η_1 and η_2 hence must be determined using the equation $\dot{\eta}_1 = \dot{\eta}_2 = L_{12}(X_1 - X_2)$ as $\eta_1 + \eta_2 = 1$ therein, and this is possible if and only if $L_{13} = L_{23} = 0$ therein within that time interval. However, if the coefficients L_{13} and L_{23} are taken as nonzero constants, the contributions from the terms $L_{13}(X_1 - X_3)$ and $L_{23}(X_2 - X_3)$ would be there unwantedly, since the driving forces $X_1 - X_3$ and $X_2 - X_3$ might be nonzero there. The desired condition can obviously be fulfilled by L_{ij} given by Eq. (2.45), but not by constant L_{ij} considered in [20]. The essence of the third and fourth conditions in Eq. (2.45) is that if variant i is absent, it cannot be transformed into other variants [55].

2.6 Boundary conditions

The boundary conditions for the phase-field equations and the mechanics problem namely the Dirichlet, Neumann, and periodic BCs are listed here.

Phase-field problem. We have applied the periodic BC for all the order parameters. If two boundaries $S_{p1\eta_k} \subset S_0$ and $S_{p2\eta_k} \subset S_0$ (where $S_{p1\eta_k} \cap S_{p2\eta_k}$ is empty), having opposite unit normals in Ω_0 , i.e. $(\mathbf{n}_0)_{S_{p1\eta_k}} = -(\mathbf{n}_0)_{S_{p2\eta_k}}$, are subjected to a periodic BC related to the order parameters η_k (for $k = 0, 1, 2, \dots, N$), then the order parameters and their gradients must satisfy

$$\eta_k|_{S_{p1\eta_k}} = \eta_k|_{S_{p2\eta_k}} \quad \text{and} \quad (\nabla_0 \eta_k \cdot \mathbf{n}_0)_{S_{p1\eta_k}} = (\nabla_0 \eta_k \cdot \mathbf{n}_0)_{S_{p2\eta_k}} \quad \text{for all } k = 0, 1, 2, \dots, N. \quad (2.48)$$

Mechanics problem. On the traction boundary $S_{0T} \subset S_0$, the traction vector is specified (denoted by \mathbf{p}^{sp}), and on the displacement boundary $S_{0u} \subset S_0$, the displacements are specified (denoted by \mathbf{u}^{sp}), i.e.

$$\mathbf{P} \cdot \mathbf{n}_0 = \mathbf{p}^{sp} \quad \text{on } S_{0T}, \quad (2.49)$$

$$\mathbf{u} = \mathbf{u}^{sp} \quad \text{on } S_{0u}. \quad (2.50)$$

If two boundaries $S_{pu1} \subset S_0$ and $S_{pu2} \subset S_0$ (where $S_{pu1} \cap S_{pu2}$ is empty) are subjected to a periodic BC on the displacements \mathbf{u} , then the displacements on these boundaries are related by

$$\mathbf{u}|_{S_{pu1}} = \mathbf{u}|_{S_{pu2}} + (\mathbf{F}_h - \mathbf{I}) \cdot \mathbf{r}_0, \quad (2.51)$$

respectively, where \mathbf{R}_1 , \mathbf{R}_2 , \mathbf{R}_3 , and \mathbf{R}_4 are the rotation tensors; \mathbf{n}_1 and \mathbf{n}_2 are the unit normals to the respective twin boundaries such that \mathbf{n}_1 points into \mathbf{M}_j and \mathbf{n}_2 points into \mathbf{M}_l (see Fig. 1); the vectors \mathbf{a}'_1 and \mathbf{a}'_2 are related to the simple shear deformations. The governing equation for the twins within twins shown in Fig. 1 is (Chapter 7 of [1] and [10, 11])

$$(\kappa_1 \mathbf{R}_2 \cdot \mathbf{U}_{tj} + (1 - \kappa_1) \mathbf{R}_1 \cdot \mathbf{U}_{ti}) - (\kappa_2 \mathbf{R}_4 \cdot \mathbf{U}_{tl} + (1 - \kappa_2) \mathbf{R}_3 \cdot \mathbf{U}_{tk}) = \mathbf{b}' \otimes \mathbf{m}, \quad (3.2)$$

where κ_1 and κ_2 are the volume fractions of \mathbf{M}_j and \mathbf{M}_k in the respective twins, \mathbf{m} is the unit normal to the twin-twin interface shown in the figure, and \mathbf{b}' is a vector related to the deformation.

Equations (3.1)₁ and (3.1)₂ can be rewritten as

$$\mathbf{Q}_1 \cdot \mathbf{U}_{tj} - \mathbf{U}_{ti} = \mathbf{a}_1 \otimes \mathbf{n}_1, \quad \text{and} \quad \mathbf{Q}_2 \cdot \mathbf{U}_{tl} - \mathbf{U}_{tk} = \mathbf{a}_2 \otimes \mathbf{n}_2, \quad (3.3)$$

where $\mathbf{Q}_1 = \mathbf{R}_1^t \cdot \mathbf{R}_2$, $\mathbf{a}_1 = \mathbf{R}_1^t \cdot \mathbf{a}'_1$, $\mathbf{Q}_2 = \mathbf{R}_3^t \cdot \mathbf{R}_4$, and $\mathbf{a}_2 = \mathbf{R}_3^t \cdot \mathbf{a}'_2$. Similarly, using Eq. (3.3)_{1,2}, Eq. (3.2) is rewritten as

$$\mathbf{Q}_3 \cdot (\mathbf{U}_{ti} + \kappa_1 \mathbf{a}_1 \otimes \mathbf{n}_1) - (\mathbf{U}_{tk} + \kappa_2 \mathbf{a}_2 \otimes \mathbf{n}_2) = \mathbf{b} \otimes \mathbf{m}, \quad (3.4)$$

where $\mathbf{Q}_3 = \mathbf{R}_3^t \cdot \mathbf{R}_1$ and $\mathbf{b} = \mathbf{R}_3^t \cdot \mathbf{b}'$. In order to solve Eq. (3.4), we post-multiply it with $(\mathbf{U}_{tk} + \kappa_2 \mathbf{a}_2 \otimes \mathbf{n}_2)^{-1}$ and rearrange the terms to rewrite the equation as [10]

$$\mathbf{Q}_3 \cdot \tilde{\mathbf{A}} = \mathbf{I} + \mathbf{b} \otimes \tilde{\mathbf{m}}, \quad (3.5)$$

where

$$\tilde{\mathbf{A}} = (\mathbf{U}_{ti} + \kappa_1 \mathbf{a}_1 \otimes \mathbf{n}_1) \cdot (\mathbf{U}_{tk} + \kappa_2 \mathbf{a}_2 \otimes \mathbf{n}_2)^{-1}, \quad \text{and} \quad \tilde{\mathbf{m}} = (\mathbf{U}_{tk} + \kappa_2 \mathbf{a}_2 \otimes \mathbf{n}_2)^{-t} \cdot \mathbf{m}. \quad (3.6)$$

The variables to be determined from the above equations (3.3) to (3.6) are κ_1 , κ_2 , δ_κ , \mathbf{a}_1 , \mathbf{a}_2 , \mathbf{n}_1 , \mathbf{n}_2 , \mathbf{b} , \mathbf{m} , \mathbf{Q}_1 , \mathbf{Q}_2 , and \mathbf{Q}_3 .

Twins within twins solution: The solution for Eq. (3.3)₁ and (3.3)₂ are well known (see e.g. Chapter 5 of [1]) and is enlisted here for completeness. To do so, we define a symmetric tensor $\mathbf{G}_1 = \mathbf{U}_{tj}^{-1} \cdot \mathbf{U}_{ti}^2 \cdot \mathbf{U}_{tj}^{-1}$ corresponding to Eq. (3.3)₁. The eigenvalues of \mathbf{G}_1 are denoted by λ_1 , λ_2 , and λ_3 , which are all positive, and the corresponding normalized eigenvectors are denoted by \mathbf{i}_1 , \mathbf{i}_2 , and \mathbf{i}_3 , respectively. Equation (3.3)₁ has a solution if and only if $\lambda_1 \leq 1$, $\lambda_2 = 1$, and $\lambda_3 \geq 1$ (assuming $\lambda_1 \leq \lambda_2 \leq \lambda_3$). The expressions for \mathbf{a}_1

and \mathbf{n}_1 are given by

$$\begin{aligned}\mathbf{a}_1 &= \zeta_1 \left(\sqrt{\frac{\lambda_3(1-\lambda_1)}{\lambda_3-\lambda_1}} \mathbf{i}_1 + \xi \sqrt{\frac{\lambda_1(\lambda_3-1)}{\lambda_3-\lambda_1}} \mathbf{i}_3 \right), \\ \mathbf{n}_1 &= \frac{\sqrt{\lambda_3}-\sqrt{\lambda_1}}{\zeta_1\sqrt{\lambda_3-\lambda_1}} \left(-\sqrt{1-\lambda_1} \mathbf{U}_{tj}\mathbf{i}_1 + \xi\sqrt{\lambda_3-1} \mathbf{U}_{tj}\mathbf{i}_3 \right)\end{aligned}\quad (3.7)$$

where $\xi = \pm 1$, and ζ_1 is such that $|\mathbf{n}_1| = 1$. The solutions \mathbf{a}_2 and \mathbf{n}_2 for the twins between \mathbf{M}_k and \mathbf{M}_l are similarly obtained using the eigenpairs of $\mathbf{U}_{tl}^{-1} \cdot \mathbf{U}_{tk}^2 \cdot \mathbf{U}_{tl}^{-1}$ in Eq. (3.7). The rotations \mathbf{Q}_1 and \mathbf{Q}_2 can then be obtained using Eqs. (3.3)_{1,2}.

We now solve the twins within twins equation (3.5) which has got a form similar to the A-twinned martensite interface equation using the procedure of Ball and James [4] (also see Chapter 7 of [10]). Noticing that the Bain stretches \mathbf{U}_{ti} , \mathbf{U}_{tj} , \mathbf{U}_{tk} , and \mathbf{U}_{tl} are given for a material, we first obtain \mathbf{a}_1 , \mathbf{a}_2 , \mathbf{n}_1 , and \mathbf{n}_2 using, e.g., Eq. (3.7). The procedure for obtaining the remaining unknowns κ_1 , κ_2 , \mathbf{Q}_3 , \mathbf{b} , and $\tilde{\mathbf{m}}$ is derived here. In obtaining these unknowns, let us first assume that the parameters κ_1 and κ_2 are given, and solve for the remaining unknown variables. We introduce

$$\mathbf{G}_2 = \tilde{\mathbf{A}}^t \cdot \tilde{\mathbf{A}}, \quad (3.8)$$

which is obviously symmetric and positive-definite, and all the eigenvalues are positive numbers which we denote by Λ_1 , Λ_2 , and Λ_3 . The corresponding normalized eigenvectors are denoted by \mathbf{j}_1 , \mathbf{j}_2 , and \mathbf{j}_3 , respectively. Equation (3.5) has a solution if and only if $\Lambda_1 \leq 1$, $\Lambda_2 = 1$, and $\Lambda_3 \geq 1$ assuming $\Lambda_1 \leq \Lambda_2 \leq \Lambda_3$. The solutions for the vectors \mathbf{b} and $\tilde{\mathbf{m}}$ are obtained as (see e.g. Chapter 6 of [1])

$$\begin{aligned}\mathbf{b} &= \frac{\zeta_2}{\sqrt{\Lambda_3-\Lambda_1}} \left(\sqrt{\Lambda_3(1-\Lambda_1)} \mathbf{j}_1 + \xi \sqrt{\Lambda_1(\Lambda_3-1)} \mathbf{j}_3 \right), \quad \text{and} \\ \tilde{\mathbf{m}} &= \frac{\sqrt{\Lambda_3}-\sqrt{\Lambda_1}}{\zeta_2\sqrt{\Lambda_3-\Lambda_1}} \left(-\sqrt{1-\Lambda_1} \mathbf{j}_1 + \xi \sqrt{\Lambda_3-1} \mathbf{j}_3 \right).\end{aligned}\quad (3.9)$$

The unit normal to the twin-twin boundary \mathbf{m} is finally obtained using Eq. (3.9)₂ in Eq. (3.6)₂

$$\mathbf{m} = \frac{\sqrt{\Lambda_3}-\sqrt{\Lambda_1}}{\zeta_2\sqrt{\Lambda_3-\Lambda_1}} (\mathbf{U}_{tk} + \kappa_2 \mathbf{n}_2 \otimes \mathbf{a}_2) \cdot \left(-\sqrt{1-\Lambda_1} \mathbf{j}_1 + \xi \sqrt{\Lambda_3-1} \mathbf{j}_3 \right), \quad (3.10)$$

where ζ_2 in Eqs. (3.9) and (3.10) is such that $|\mathbf{m}| = 1$. The rotation \mathbf{Q}_3 is then determined using Eqs. (3.9)_{1,2} in Eq. (3.5). Note that the middle eigenvalues Λ_2 obtained would be an expression as a function of the volume fractions κ_1 and κ_2 . Setting $\Lambda_2 = 1$, which is required for the existence of the twins within twins solution [10], would give a relation between κ_1 and κ_2 . However, it is not possible to obtain the exact solutions for κ_1 and κ_2 from the limited governing equations at hand. The thickness of the transition layer κ_t is also indeterminate.

3.2 Twins within twins solutions for cubic to tetragonal MTs

The solutions for twins within twins for cubic to tetragonal MTs are now obtained. The three Bain stretch tensors for such transformations are [1]

$$\begin{aligned} \mathbf{U}_{t1} &= \chi \mathbf{c}_1 \otimes \mathbf{c}_1 + \alpha \mathbf{c}_2 \otimes \mathbf{c}_2 + \alpha \mathbf{c}_3 \otimes \mathbf{c}_3, \\ \mathbf{U}_{t2} &= \alpha \mathbf{c}_1 \otimes \mathbf{c}_1 + \chi \mathbf{c}_2 \otimes \mathbf{c}_2 + \alpha \mathbf{c}_3 \otimes \mathbf{c}_3, \\ \mathbf{U}_{t3} &= \alpha \mathbf{c}_1 \otimes \mathbf{c}_1 + \alpha \mathbf{c}_2 \otimes \mathbf{c}_2 + \chi \mathbf{c}_3 \otimes \mathbf{c}_3, \end{aligned} \quad (3.11)$$

where $\alpha < 1$ and $\chi > 1$ are the material constants and $\{\mathbf{c}_1, \mathbf{c}_2, \mathbf{c}_3\}$ is a right-handed standard Cartesian basis in the cubic unit cell of **A** such that the basis vectors are parallel to three mutually orthogonal sides of that unit cell. The solutions for twins between **M**₁-**M**₂ (**n** pointing into **M**₂), **M**₁-**M**₃ (**n** pointing into **M**₃), and **M**₂-**M**₃ (**n** pointing into **M**₃) are (see e.g. Chapter 5 of [1])

$$\begin{aligned} \mathbf{a} &= \sqrt{2}v(-\chi \mathbf{c}_1 \pm \alpha \mathbf{c}_2), & \mathbf{n} &= (\mathbf{c}_1 \pm \mathbf{c}_2)/\sqrt{2}; \\ \mathbf{a} &= \sqrt{2}v(-\chi \mathbf{c}_1 \pm \alpha \mathbf{c}_3), & \mathbf{n} &= (\mathbf{c}_1 \pm \mathbf{c}_3)/\sqrt{2}; \\ \mathbf{a} &= \sqrt{2}v(-\chi \mathbf{c}_2 \pm \alpha \mathbf{c}_3), & \mathbf{n} &= (\mathbf{c}_2 \pm \mathbf{c}_3)/\sqrt{2}, \end{aligned} \quad (3.12)$$

respectively, where $v = (\chi^2 - \alpha^2)/(\chi^2 + \alpha^2)$. Since all the variants for tetragonal **M** phase are in a twin relationship [1], the combinations of possible twins within twins solutions are $\{\mathbf{M}_1, \mathbf{M}_2\}$ - $\{\mathbf{M}_1, \mathbf{M}_3\}$, $\{\mathbf{M}_2, \mathbf{M}_1\}$ - $\{\mathbf{M}_2, \mathbf{M}_3\}$, and $\{\mathbf{M}_2, \mathbf{M}_3\}$ - $\{\mathbf{M}_2, \mathbf{M}_1\}$, where the corresponding twin solutions $\{\mathbf{a}_1, \mathbf{n}_1\}$ and $\{\mathbf{a}_2, \mathbf{n}_2\}$ are to be considered from Eq. (3.12).

Using Eq. (3.6)₁ and the solutions to the corresponding twin pairs from Eq. (3.12), we get **G**₂ as the following diagonal tensor for all the possible combinations of twins within twins listed above:

$$\mathbf{G}_2 = \tilde{\mathbf{A}}^t \cdot \tilde{\mathbf{A}} = \Lambda_1 \mathbf{j}_1 \otimes \mathbf{j}_1 + \Lambda_2 \mathbf{j}_2 \otimes \mathbf{j}_2 + \Lambda_3 \mathbf{j}_3 \otimes \mathbf{j}_3, \quad \text{where} \quad (3.13)$$

$$\begin{aligned} \Lambda_1 &= [1 - \kappa_2 v]^2 < 1, \\ \Lambda_2 &= [(1 + \kappa_1)\alpha^2 + (1 - \kappa_1)\chi^2]^2 [(1 + \kappa_2)\chi^2 + (1 - \kappa_2)\alpha^2]^2 / (\chi^2 + \alpha^2)^4 = 1, \quad \text{and} \\ \Lambda_3 &= [1 + \kappa_1 v]^2 > 1, \end{aligned} \quad (3.14)$$

and we have used the facts $\chi > 1$, $\alpha < 1$, $0 < v < 1$, and $0 < \kappa_1, \kappa_2 < 1$. The eigenvectors **j**₁, **j**₂, and **j**₃ are functions of the vectors **c**₁, **c**₂, and **c**₃ and depend on the combinations of the variants in the twins as obtained below. We have imposed the condition $\Lambda_2 = 1$ in Eq. (3.14)₂, which is a requirement for **G**₂

given by Eq. (3.13) to represent a twins within twins as discussed above, and from that the following two conditions on the parameters χ , α , κ_1 , κ_2 are obtained:

$$\begin{aligned} \frac{1}{\kappa_1} - \frac{1}{\kappa_2} &= v, \quad \text{or} \\ (\kappa_1 - \kappa_2) \frac{1}{v} + \kappa_1 \kappa_2 &= \frac{2}{v^2}. \end{aligned} \quad (3.15)$$

Since $0 < v < 1$, Eq. (3.15)₁ is satisfied if and only if $\kappa_1 < \kappa_2$. For $\kappa_1 = \kappa_2$ Eq. (3.15)₁ yields the trivial condition $\chi = \alpha$ which does not yield twins within twins. It is easy to verify that for all $\chi > 1$ and $\alpha < 1$ no $0 < \kappa_1, \kappa_2 < 1$ satisfy Eq. (3.15)₂, and hence we disregard this relation. Finally, considering κ_1 and κ_2 are related by Eq. (3.15)₁, and using the expressions for Λ_1 and Λ_3 given by Eqs. (3.14)_{1,3} into Eqs. (3.7) and (3.10), we get the solutions for \mathbf{b} and \mathbf{m} for different twins within twins as listed below.

Case I For $\{\mathbf{M}_1, \mathbf{M}_2\}$ - $\{\mathbf{M}_1, \mathbf{M}_3\}$ twin pairs

For $\{\mathbf{M}_1, \mathbf{M}_2\}$ - $\{\mathbf{M}_1, \mathbf{M}_3\}$ twin pairs the indices are $i = k = 1$, $j = 2$, and $l = 3$, and κ_1 and κ_2 are the volume fractions of \mathbf{M}_1 in the respective twins. The eigenvectors of \mathbf{G}_2 tensor are obtained as $\mathbf{j}_1 = \mathbf{c}_3$, $\mathbf{j}_2 = \mathbf{c}_1$, and $\mathbf{j}_3 = \mathbf{c}_2$. The vectors \mathbf{b} and $\tilde{\mathbf{m}}$ are obtained using Eqs. (3.14)_{1,3} in Eq. (3.9) as

$$\begin{aligned} \mathbf{b} &= \frac{\zeta_2}{\sqrt{(\kappa_1 + \kappa_2)[2 + (\kappa_1 - \kappa_2)v]}} \left[\xi(1 - \kappa_2 v) \sqrt{\kappa_1(2 + \kappa_1 v)} \mathbf{c}_2 + (1 + \kappa_1 v) \sqrt{\kappa_2(2 - \kappa_2 v)} \mathbf{c}_3 \right], \quad \text{and} \\ \tilde{\mathbf{m}} &= \frac{\sqrt{\kappa_1 + \kappa_2} v}{\zeta_2 \sqrt{2 + (\kappa_1 - \kappa_2)v}} \left[\xi \sqrt{\kappa_1(2 + \kappa_1 v)} \mathbf{c}_2 - \sqrt{\kappa_2(2 - \kappa_2 v)} \mathbf{c}_3 \right], \end{aligned} \quad (3.16)$$

respectively. Using Eq. (3.16)₂ and (3.7) in Eq. (3.10) we finally get \mathbf{m} as

$$\mathbf{m} = \frac{\sqrt{\kappa_1 + \kappa_2} v \alpha}{\zeta_2 \sqrt{2 + (\kappa_1 - \kappa_2)v}} \left[-v \kappa_2^{1.5} \sqrt{2 - \kappa_2 v} \mathbf{c}_1 + \xi \sqrt{\kappa_1(2 + \kappa_1 v)} \mathbf{c}_2 + \sqrt{\kappa_2(2 - \kappa_2 v)} (1 + \kappa_2 v) \mathbf{c}_3 \right], \quad (3.17)$$

where the condition $|\mathbf{m}| = 1$ yields

$$\zeta_2 = \frac{\sqrt{\kappa_1 + \kappa_2} v \alpha}{\sqrt{2 + (\kappa_1 - \kappa_2)v}} \left[\kappa_2(2 - \kappa_2 v)(1 + 2\kappa_2 v + 2\kappa_2^2 v^2) + \kappa_1(2 + \kappa_1 v) \right]. \quad (3.18)$$

Case II For $\{\mathbf{M}_2, \mathbf{M}_1\}$ - $\{\mathbf{M}_2, \mathbf{M}_3\}$ twin pairs

In this case the indices are $i = k = 2$, $j = 1$, and $l = 3$, and κ_1 and κ_2 are the volume fractions of \mathbf{M}_2 in the respective twins. The eigenvectors for \mathbf{G}_2 tensor are given by $\mathbf{j}_1 = \mathbf{c}_3$, $\mathbf{j}_2 = \mathbf{c}_2$, and $\mathbf{j}_3 = \mathbf{c}_1$. The vectors \mathbf{b} and $\tilde{\mathbf{m}}$ are obtained using Eqs. (3.7) and (3.9) as

$$\begin{aligned} \mathbf{b} &= \frac{\zeta_2}{\sqrt{(\kappa_1 + \kappa_2)[2 + (\kappa_1 - \kappa_2)v]}} \left[(1 + \kappa_1 v) \sqrt{\kappa_2(2 - \kappa_2 v)} \mathbf{c}_3 + \xi(1 - \kappa_2 v) \sqrt{\kappa_1(2 + \kappa_1 v)} \mathbf{c}_1 \right], \quad \text{and} \\ \tilde{\mathbf{m}} &= \frac{\sqrt{\kappa_1 + \kappa_2} v}{\zeta_2 \sqrt{2 + (\kappa_1 - \kappa_2)v}} \left[-\sqrt{\kappa_2(2 - \kappa_2 v)} \mathbf{c}_3 + \xi \sqrt{\kappa_1(2 + \kappa_1 v)} \mathbf{c}_1 \right], \end{aligned} \quad (3.19)$$

respectively. Using Eq. (3.16)₂ in Eq. (3.10) we finally get \mathbf{m} as

$$\mathbf{m} = \frac{\sqrt{\kappa_1 + \kappa_2} v \alpha}{\zeta_2 \sqrt{2 + (\kappa_1 - \kappa_2)v}} \left[-\xi v \kappa_2^{1.5} \sqrt{2 - \kappa_2 v} \mathbf{c}_2 + \xi \sqrt{\kappa_1(2 + \kappa_1 v)} \mathbf{c}_1 + \sqrt{\kappa_2(2 - \kappa_2 v)}(1 + \kappa_2 v) \mathbf{c}_3 \right] \quad (3.20)$$

where ζ_2 is given by Eq. (3.18).

Case III For $\{M_3, M_1\}$ - $\{M_3, M_2\}$ twin pairs

In this case the indices are $i = k = 3$, $j = 1$, and $l = 2$, and κ_1 and κ_2 are the volume fractions of M_3 in the respective twins. The eigenvectors for \mathbf{G}_2 tensor are given by $\mathbf{j}_1 = \mathbf{c}_2$, $\mathbf{j}_2 = \mathbf{c}_3$, and $\mathbf{j}_3 = \mathbf{c}_1$. The vectors \mathbf{b} and $\tilde{\mathbf{m}}$ are obtained using Eqs. (3.7) and (3.10) as

$$\begin{aligned} \mathbf{b} &= \frac{\zeta_2}{\sqrt{(\kappa_1 + \kappa_2)[2 + (\kappa_1 - \kappa_2)v]}} \left[(1 + \kappa_1 v) \sqrt{\kappa_2(2 - \kappa_2 v)} \mathbf{c}_2 + \xi(1 - \kappa_2 v) \sqrt{\kappa_1(2 + \kappa_1 v)} \mathbf{c}_1 \right], \quad \text{and} \\ \tilde{\mathbf{m}} &= \frac{\sqrt{\kappa_1 + \kappa_2} v}{\zeta_2 \sqrt{2 + (\kappa_1 - \kappa_2)v}} \left[-\sqrt{\kappa_2(2 - \kappa_2 v)} \mathbf{c}_2 + \xi \sqrt{\kappa_1(2 + \kappa_1 v)} \mathbf{c}_1 \right], \end{aligned} \quad (3.21)$$

respectively. Using Eq. (3.16)₂ in Eq. (3.10) we finally get \mathbf{m} as

$$\mathbf{m} = \frac{\sqrt{\kappa_1 + \kappa_2} v \alpha}{\zeta_2 \sqrt{2 + (\kappa_1 - \kappa_2)v}} \left[-\xi v \kappa_2^{1.5} \sqrt{2 - \kappa_2 v} \mathbf{c}_3 + \xi \sqrt{\kappa_1(2 + \kappa_1 v)} \mathbf{c}_1 + \sqrt{\kappa_2(2 - \kappa_2 v)}(1 + \kappa_2 v) \mathbf{c}_2 \right] \quad (3.22)$$

where ζ_2 is given by Eq. (3.18).

In summary, we have obtained the general analytical solution for \mathbf{a}_1 , \mathbf{a}_2 , \mathbf{n}_1 , \mathbf{n}_2 , \mathbf{b} , and \mathbf{m} listed in Eqs. (3.7), (3.9), and (3.10). The rotation tensors \mathbf{Q}_1 , \mathbf{Q}_2 , and \mathbf{Q}_3 can be finally obtained using Eqs. (3.4)_{1,2} and (3.3). The twins within twins solutions for cubic to tetragonal MTs are listed in Eqs. (3.12) and (3.16) to (3.22). Since the volume fractions κ_1 and κ_2 satisfy the relation given by Eq. (3.15)₁, there are obviously many solutions possible for each of the twins within twins listed in Cases (I), (II) and (III) (also see Chapter 7 of [1]). The width of the twins within twins interface (shaded region in Fig. 1) δ_κ is indeterminate within the set of governing equations at hand.

4 Results and discussions

We now present the simulation results for twins within twins microstructure obtained using our phase-field approach. The materials properties for NiAl alloy, which exhibits cubic to tetragonal MTs, are considered and listed in Section 4.1. In Section 4.2 the phase-field results are compared with the crystallographic solution obtained in Section 3.

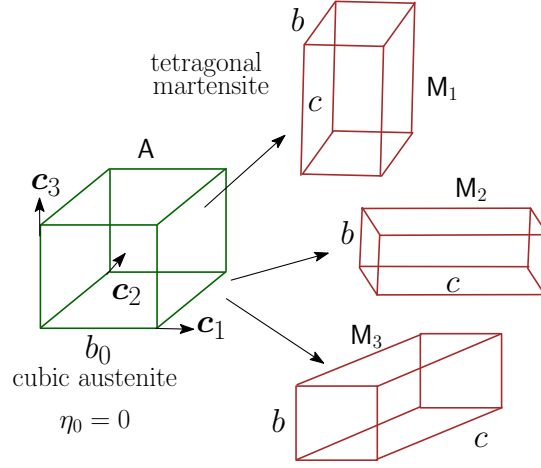


Figure 2: Unit cells for cubic austenite and three tetragonal martensitic variants.

4.1 Material parameters

The material parameters for NiAl alloy are enlisted here. We consider the interfacial widths and energies as $\delta_{0M} = 1$ nm, $\gamma_{0M} = 0.2$ N/m, $\delta_{12} = \delta_{13} = \delta_{23} = 0.75$ nm, and $\gamma_{12} = \gamma_{13} = \gamma_{23} = 0.1$ N/m. Using the following analytical relations between the interfacial thickness and energy, and the phase-field parameters [67, 72]

$$\delta_{ij} = \sqrt{18\beta_{ij}/A_{ij}}; \quad \beta_{ij} = \gamma_{ij}\delta_{ij} \quad \text{for A-M and all the variant-variant interfaces,} \quad (4.1)$$

which were obtained by solving an 1D Ginzburg-Landau equation neglecting mechanics, we obtain $\rho_0 A_{0M} = 3600$ MPa, $\rho_0 \bar{A} = 2400$ MPa, $\beta_{0M} = 2 \times 10^{-10}$ N, and $\beta_{12} = \beta_{13} = \beta_{23} = 7.5 \times 10^{-11}$ N. We take $\theta_e = 215$ K and $\Delta s = -1.47$ MPa K⁻¹, using which we calculate the critical temperatures for A \rightarrow M and M \rightarrow A transformations as (see [59]) $\theta_{A \rightarrow M}^c = \theta_e + A_{0M}/(3\Delta s) = 0$ K and $\theta_{M \rightarrow A}^c = \theta_e - A_{0M}/(3\Delta s) = 430$ K, respectively. The Lamé constants assuming isotropic elasticity are taken to be identical for all the phases A, M₁, M₂, and M₃: $\lambda_0 = \lambda_1 = \lambda_2 = \lambda_3 = 74.62$ GPa, $\mu_0 = \mu_1 = \mu_2 = \mu_3 = 72$ GPa. The other material constants are taken as $a_\beta = a_\varepsilon = a_K = 3$, $a_0 = 10^{-3}$, $K_{12} = K_{23} = K_{13} = 50$ GPa, $K_{012} = K_{023} = K_{013} = 5$ GPa, $K_{0123} = K_{123} = 50$ GPa, $L_{0M} = 2600$ (Pa-s)⁻¹ and $L_{12} = L_{13} = L_{23} = 12600$ (Pa-s)⁻¹. The transformation stretches are $\alpha = 0.922$ and $\chi = 1.215$ [45].

4.2 Numerical result for twins within twins

For the simulation we consider a 22 nm \times 22 nm \times 22 nm cube as the reference configuration Ω_0 as shown in Figs. 3(a). The periodic BCs given by Eq. (2.48) are used for all the order parameters on the

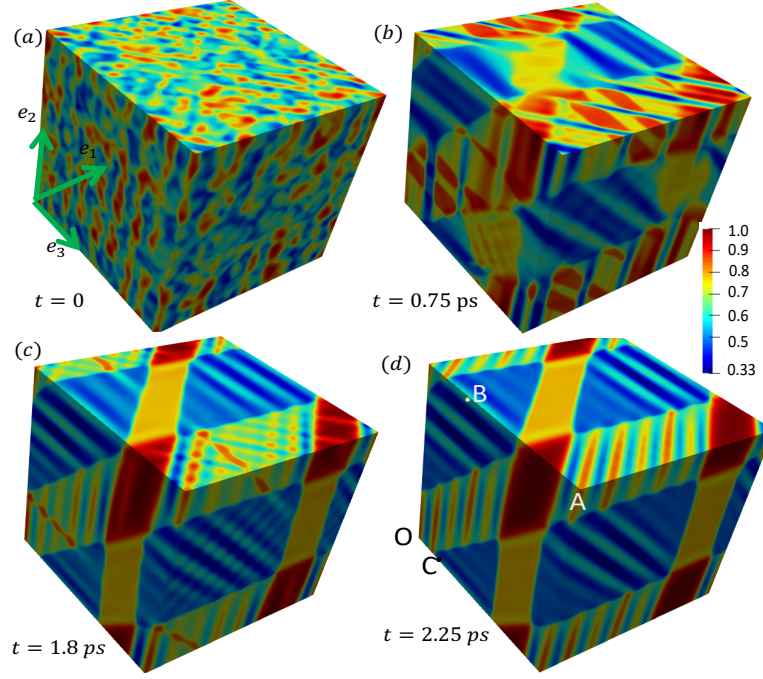


Figure 3: Evolution of twin within twin microstructure in a $22 \text{ nm} \times 22 \text{ nm} \times 22 \text{ nm}$ cube shown by color plot of $\eta_{eq} = \eta_0(1 - 0.67\eta_1 - 0.33\eta_2)$: $\eta_{eq} = 0.33$ denotes M_1 ; $\eta_{eq} = 0.67$ denotes M_2 ; $\eta_{eq} = 1$ denotes M_3 .

respective opposite faces of the cube domain. We have used the periodic BC for the normal component of the displacement vector on the opposite faces of the cube given by Eq. (2.51) with the homogeneous deformation gradient as $\mathbf{F}_h = \mathbf{I} + 0.98 \mathbf{n}_0 \otimes \mathbf{n}_0$, where \mathbf{n}_0 is the unit normal to the opposite faces of the cube in Ω_0 . On each face of the cube domain, we have used the traction-free BC for the tangential components of the first Piola-Kirchhoff traction vector. The temperature of the sample is taken as $\theta = 0$ K. The material properties listed in Section 4.1 are used. The Bain tensors listed in Eq. (3.11) are used in Eq. (2.5), where the basis vectors \mathbf{c}_1 , \mathbf{c}_2 , and \mathbf{c}_3 of A unit cell are parallel to basis vectors \mathbf{e}_1 , \mathbf{e}_2 , and \mathbf{e}_3 , respectively, attached to the sample (see Fig. 3 (a)). The initial distribution of the order parameters are taken between $0 \leq \eta_0 \leq 1$, $0 \leq \eta_1 \leq 0.8$, and $0 \leq \eta_2 \leq 0.8$, all distributed randomly shown in Figs. 3(a). The other order parameter η_3 is calculated using Eq. (2.1) for all the times $t \geq 0$. We have used a finite element procedure similar to that of [73] developed by the authors. A finite element code has been developed using an open-source code deal.ii [74]. The domain is discretized spatially with quadratic brick element and it is ensured that at least three grid points lie across all the interfaces. The mesh density in the 3D domain is shown in Fig. 4(a), and the mesh density on one of the boundaries is shown in Fig. 4(b). The time derivatives of the order parameters are discretized using the backward difference scheme of order two described in [73]. A constant time step size of 2×10^{-16} s is used for the simulation.

The evolution of the microstructure is shown at different time instances in Figs. 3. We have in fact

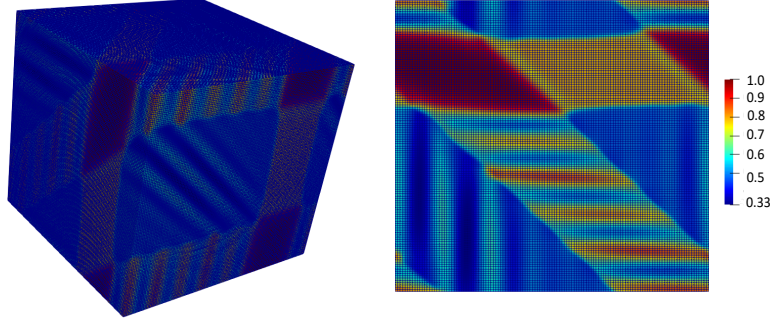


Figure 4: (a) Mesh density in the 3D computational domain. (b) Mesh density on one of the external boundaries.

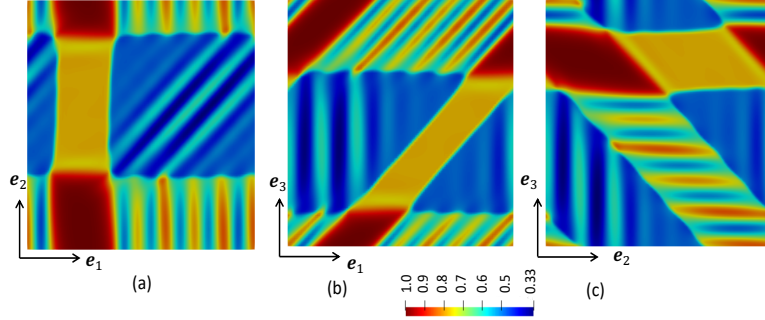


Figure 5: The twin microstructures on three mutually perpendicular faces of the sample shown in Fig. 3. The colour plots of η_{eq} are shown: $\eta_{eq} = 0.33$ denotes M_1 ; $\eta_{eq} = 0.67$ denotes M_2 ; $\eta_{eq} = 1$ denotes M_3 .

shown a colour plot for an equivalent order parameter defined as $\eta_{eq} = \eta_0(1 - 0.67\eta_1 - 0.33\eta_2)$ which obviously takes the following values in different phases: $\eta_{eq} = 0$ in A, $\eta_{eq} = 0.33$ in M_1 , $\eta_{eq} = 0.67$ in M_2 , and $\eta_{eq} = 1$ in M_3 . Figure 3(a) shows the initial distribution of η_{eq} . Figures 3(b) and (c) show the intermediate microstructures at different time instances which are approaching a twinned microstructure. We finally obtain twins within twins microstructures between the twin pairs M_1 - M_2 and M_1 - M_3 as shown in Fig. 3(d). The microstructure shown in Fig. 3(d) is a little far from being a stationary one. However, the twinned microstructure obtained can be compared with the analytical solution as there is no further significant change in the orientations of the twin boundaries and twin-twin boundaries with time as observed in Figs. 3 (c) and (d). The microstructures on three faces of the domain with unit normals parallel to e_3 , e_2 and e_1 are shown in Fig. 5(a), (b), and (c), respectively.

The plots for the components of the Cauchy elastic stress tensor (in GPa) at $t = 2.25$ ps (corresponding to the microstructure shown in Fig. 3 (d)) are shown in Fig. 6. The internal stresses are concentrated mainly across the twin-twin boundaries and also across the twin boundaries (see e.g. [75] for experimental results). The stresses vary from compressive to tensile between two adjacent variant plates within and near the twin-twin interfaces. For a better understanding of the elastic stresses across the interfaces,

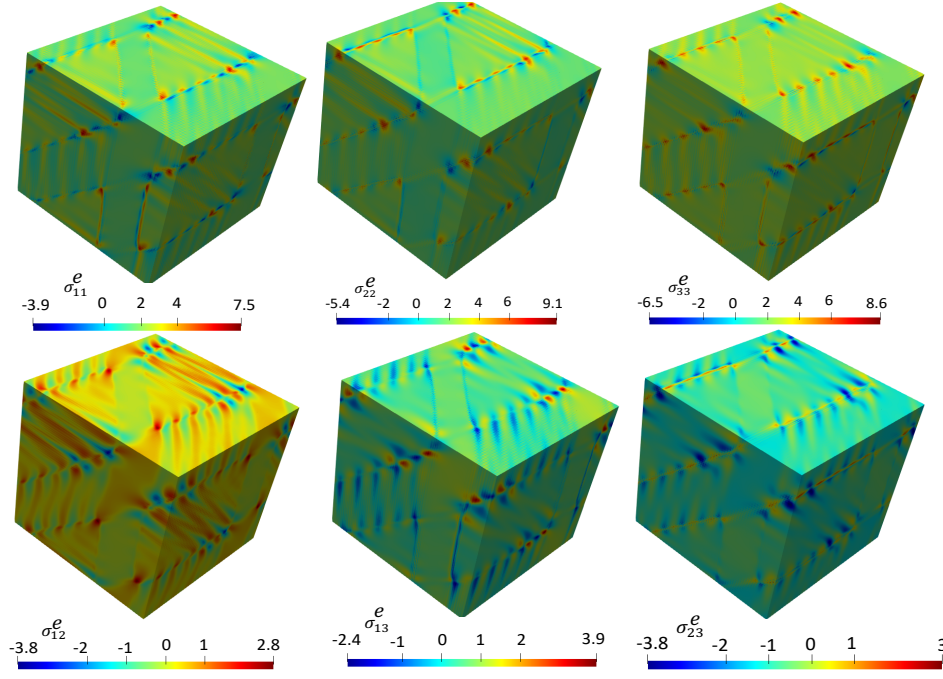


Figure 6: Components of the Cauchy elastic stress tensor (in GPa) in the domain shown in Fig. 3(d).

Table-1: Crystallographic solutions for twins between the variants for NiAl alloy in $\{\mathbf{c}_1, \mathbf{c}_2, \mathbf{c}_3\}$ basis.

Variant pair	\mathbf{a}	\mathbf{n}
M ₁ -M ₂	$-0.4625 \mathbf{c}_1 \pm 0.3510 \mathbf{c}_2$	$0.7071 \mathbf{c}_1 \pm 0.7071 \mathbf{c}_2$
M ₂ -M ₃	$0.4625 \mathbf{c}_1 \pm 0.3510 \mathbf{c}_3$	$-0.7071 \mathbf{c}_1 \pm 0.7071 \mathbf{c}_3$
M ₃ -M ₁	$0.4625 \mathbf{c}_2 \pm 0.3510 \mathbf{c}_3$	$-0.7071 \mathbf{c}_2 \pm 0.7071 \mathbf{c}_3$

we have shown a plot for the components across the lines joined by the points O and A, and C and B (see Fig. 3 (d)) in Fig. 7(a) and (b), respectively. Obviously, in these two figures, the elastic stresses within M₁-M₃ and M₁-M₂ twin boundaries are plotted. Figure 7(b) also shows the stresses across a twin-twin boundary. All the normal stresses $\sigma_{(e)11}$, $\sigma_{(e)22}$, and $\sigma_{(e)33}$ are significantly higher across the twin boundaries compared to the adjacent phases. The reason for such large elastic stresses within the twin boundaries is studied in detail by the authors in [76]. The shear stresses $\sigma_{(e)12}$ and $\sigma_{(e)13}$ on the corresponding external boundary (having unit normal \mathbf{e}_1 in Ω_0) are much lower due to the traction-free BC applied in the tangential plane. From the elastic stress plots shown in Fig. 6 it is clear that stresses are mainly concentrated within the twin boundaries and the twins-twins boundaries. In fact, the stresses within twins within twins boundaries are usually much higher than that across the twin boundaries (also see Fig. 7). This can be justified by noticing that the twin-twin boundaries are compatible in an average sense, whereas the twin boundaries are compatible in Hadamard's sense according to the crystallographic theory (see Chapter 5 of [1]). Understanding the stress distributions across these interfaces is important from the materials design perspective [75].

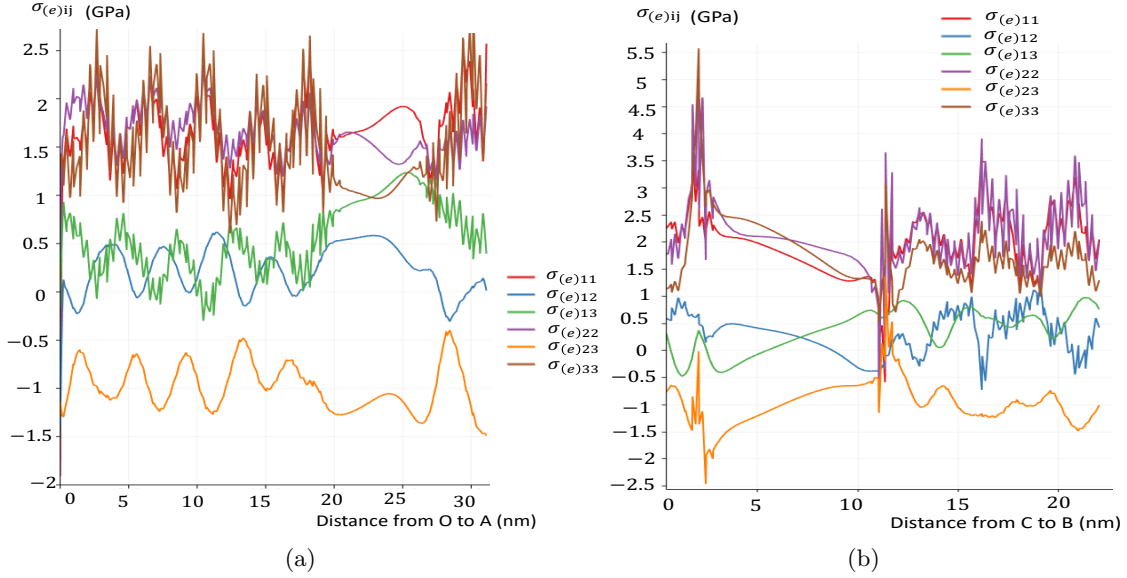


Figure 7: Components of the Cauchy elastic stress tensor across the lines drawn between points (a) O and A, and (b) C and B shown in Fig. 3(d). Obviously, figures (a) and (b) show the elastic stress distribution across the twin boundaries between variants M_1 - M_3 and M_1 - M_2 , respectively.

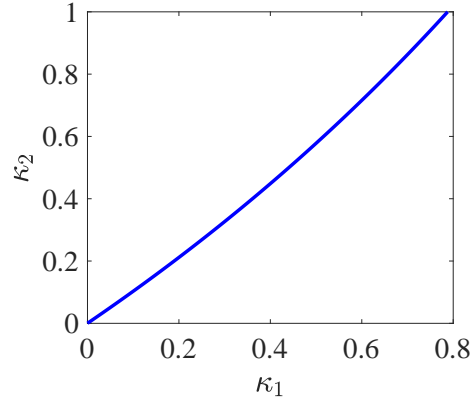


Figure 8: Plot for κ_2 versus κ_1 given by Eq. (3.15)₁ for NiAl alloy.

Comparison of crystallographic and numerical solutions. We now present a comparative study of the microstructure obtained numerically with the crystallographic solution given in Section 3.2. We have shown in Fig. 3 the twins within twins microstructures obtained using the present phase-field approach, where a twin with a variant pair M_1 - M_2 is forming interfaces with another twin made of variants pair M_1 - M_3 , i.e. the indices of Fig. 1 are $i = k = 1$, $j = 2$, and $l = 3$. The normal to the interfaces between M_1 and M_2 plates are making approximately 45° with both e_1 and e_2 axes, and the normal to the interfaces between M_1 and M_3 plates are making approximately 45° with both e_2 and e_3 axes. The normals to these twins are obviously in good agreement with the crystallographic solution listed in Table-1. The volume fractions of M_1 in the respective twin pairs are calculated as $\kappa_1 = 0.46$ and $\kappa_2 = 0.56$. The unit normal

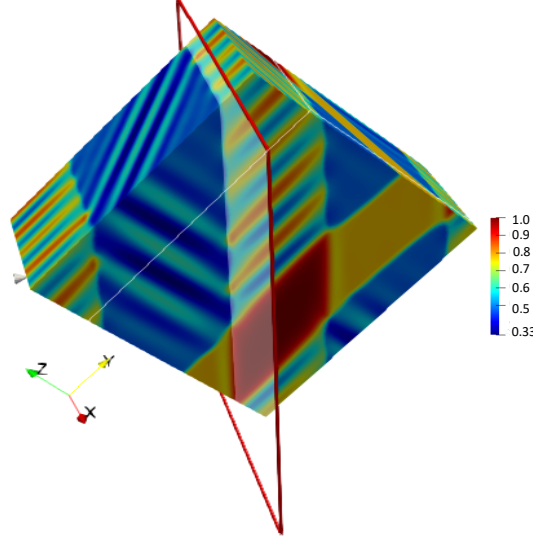


Figure 9: A plane within a twins within twins interface (within the domain shown in Fig. 3(d)) is shown by the rectangle. The unit normal to that plane is $\mathbf{m} = 0.1020 \mathbf{c}_1 - 0.7204 \mathbf{c}_2 + 0.6859 \mathbf{c}_3$.

to one of the twins within twins interface \mathbf{m} is obtained as

$$\mathbf{m} = 0.1020 \mathbf{c}_1 - 0.7204 \mathbf{c}_2 + 0.6859 \mathbf{c}_3, \quad (4.2)$$

where a rectangular plane (on red lines) lying on the twin-twin interface is shown in Fig. 9. We now calculate the analytical expression for \mathbf{m} . As mentioned earlier, the volume fractions κ_1 and κ_2 , satisfying the relation given by Eq. (3.15)₁ and plotted in Fig. 8, cannot be uniquely determined from the limited governing equations at hand. In view of that, we simply assume $\kappa_1 = 0.46$ for the analytical solution and obtain $\kappa_2 = 0.5250$ using Eq. (3.15)₁ which differs from the numerical result by 7.7%. Finally, using Eqs. (3.16), (3.17), and (3.18) we obtain $\zeta_2 = 0.2634$ and the vectors \mathbf{b} , $\tilde{\mathbf{m}}$, and \mathbf{m} as

$$\begin{aligned} \mathbf{b} &= \pm 0.1362 \mathbf{c}_2 + 0.2093 \mathbf{c}_3, \\ \tilde{\mathbf{m}} &= \pm 0.7119 \mathbf{c}_2 - 0.7115 \mathbf{c}_3, \quad \text{and} \\ \mathbf{m} &= -0.0928 \mathbf{c}_1 \pm 0.6560 \mathbf{c}_2 + 0.7492 \mathbf{c}_3. \end{aligned} \quad (4.3)$$

The maximum difference in the components of analytical and numerically obtained unit normals \mathbf{m} is within 10%, and the orientation of the analytical \mathbf{m} differs by 12.3° from the numerical one, which is acceptable. One of the main sources of difference is that in the numerical solution local stress fields and their relaxation by incomplete martensitic variants at the twin within twin interface is automatically taken into account.

5 Concluding remarks

A thermodynamically consistent Ginzburg-Landau type nanoscale multiphase phase-field approach to multivariant martensitic transformations is formulated at large strain and taking the interfacial stresses into consideration. A total of N independent order parameters are assumed to describe the austenite and N martensitic variants. A non-contradictory form for the gradient energy is considered, and the gradient energies with the previous models are compared. Furthermore, a non-contradictory kinetic model for the coupled Ginzburg-Landau equations is derived for all the order parameters. The kinetic models from the previous models are compared and their shortcomings are discussed. A general crystallographic solution for the twins within twins microstructure is obtained, and the solutions for cubic to tetragonal transformations are presented. Using the present phase-field approach 3D twins within twins microstructures evolution in a single grain is studied, and the numerical results are compared with the crystallographic solution. The present phase-field model can be used for studying more complex microstructures with more variants such as cubic \leftrightarrow orthorhombic and cubic \leftrightarrow monoclinic MTs, and also in polycrystalline solids. Note that for large transformation strains for the MTs Si I to Si II, a new martensitic microstructure, which does not obey the mathematical theory of martensite [1–5], was obtained with molecular dynamic simulations in [77]. It will be a challenge for the current (and any other) large-strain theory to reproduce such a microstructure.

Acknowledgments

AB acknowledges the support from SERB, Government of India (Project number SRG/2020/001194), and IIT Tirupati. VL acknowledges the support from NSF (CMMI-1943710 and DMR-1904830) and Iowa State University (Vance Coffman Faculty Chair Professorship). The simulations were performed at Extreme Science and Engineering Discovery Environment (XSEDE), allocations TG-MSS140033 and MSS170015.

References

- [1] K. Bhattacharya, Microstructure of Martensite: Why It Forms and How It Gives Rise to the Shape-Memory Effect, Oxford University Press, Oxford, 2004.
- [2] M. Pitteri, G. Zanzotto, Continuum Models for Phase Transitions and Twinning in Crystals, Chapman & Hall/CRC, Boca Raton, 2003.

- [3] K. Adachi, C.M. Wayman, Transformation behavior of nearly stoichiometric Ni-Mn alloy, *Metall. Trans. A* 16 (1985) 1567-1579.
- [4] J.M. Ball, R.D. James, Fine Phase Mixtures as Minimizers of Energy, *Arch. Ration. Mech. Anal.* 100 (1987) 13-52.
- [5] K.Bhattacharya, Wedge-like microstructure in martensites, *Acta Metall. Mater.* 39 (1991) 2431-2444.
- [6] D.A. Porter, K.E. Easterling, M.Y. Sherif, *Phase Transformations in Metals and Alloys*. CRC Press, Boca Raton, (2000).
- [7] J. Wang, P. Steinmann, On the modeling of equilibrium twin interfaces in a single-crystalline magnetic shape memory alloy sample. I: theoretical formulation, *Continuum Mech. Thermodyn.* 26 (2014) 563-592.
- [8] S. Govindjee, K. Hackl, R. Heinen, An upper bound to the free energy of mixing by twin-compatible lamination for n -variant martensitic phase transformations, *Continuum Mech. Thermodyn.* 18 (2007) 443-453.
- [9] D. Schryvers, P. Boullaya, P. L. Potapov, R.V. Kohn, J.M. Ball, Microstructures and interfaces in Ni-Al martensite: comparing HRTEM observations with continuum theories, *Int. J. Solids Struct.* 39 (2002) 3543-3554.
- [10] C. Chu, Hysteresis and microstructures: a study of biaxial loading on compound twins of copper-aluminum-nickel single crystals. PhD Dissertation, University of Minnesota (1993).
- [11] R. Abeyaratne, C. Chu, R.D. James, Kinetics of materials with wiggly energies: Theory and application to the evolution of twinning microstructures in a Cu-Al-Ni shape memory alloy. *Philos. Mag. A* 73 (1996) 457-497.
- [12] D. Schryvers, D. Holland-Moritz, Austenite and martensite microstructures in splat-cooled Ni-Al, *Intermetallics*, 6 (1998) 427-436.
- [13] R.D. James, K.F. Hane. Martensitic transformations and shape memory materials, *Acta Mater.* 48 (2000) 197-222.
- [14] K.F. Hane, T.W. Shield, Microstructure in a copper-aluminium-nickel shape-memory alloy, *Proc. R. Soc. Lond. A* 455 (1999) 3901-3915.

- [15] G. Ruddock, A microstructure of martensite which is not a minimiser of energy: the X-interface, *Arch. Rat. Mech. Anal.* 127 (1994) 1-39.
- [16] S. Stupkiewicz, A.G. Lengiewicz, Almost compatible X-microstructures in CuAlNi shape memory alloy, *Continuum Mech. Thermodyn.* 24 (2012) 149-164.
- [17] A. Umantsev, *Field Theoretic Method in Phase Transformations*, Springer, Heidelberg, 2012.
- [18] S.M. Allen, J.W. Cahn, A microscopic theory for antiphase boundary motion and its application to antiphase domain coarsening, *Acta Mater.* 27 (1979) 1085-1095.
- [19] Y.M. Jin, A. Artemev, A.G. Khachaturyan, Three-dimensional phase field model of low-symmetry martensitic transformation in polycrystal: Simulation of ζ_2 martensite in AuCd alloys, *Acta Mater.* 49 (2001) 2309-2320.
- [20] A. Basak, V.I. Levitas, Nanoscale multiphase phase field approach for stress- and temperature-induced martensitic phase transformations with interfacial stresses at finite strains, *J. Mech. Phys. Solids* 113 (2018) 162-196.
- [21] V.A. Levin, V.I. Levitas, K.M. Zingerman, E.I. Freiman, Phase-field simulation of stress-induced martensitic phase transformations at large strains, *Int. J. Solids Struct.* 50 (2013) 2914-2928.
- [22] K. Tuma, M. R. Hajidehib, J. Hrona, P.E. Farrell, S. Stupkiewicz, Phase field modeling of multivariant martensitic transformation at finite-strain: Computational aspects and large-scale finite-element simulations, *Comput. Methods Appl. Mech. Engrg.* 377 (2021) 113705.
- [23] A. Artemev, Y. Wang, A.G. Khachaturyan, Three-dimensional phase field model and simulation of martensitic transformation in multilayer systems under applied stresses, *Acta. Mater.* 48 (2000) 2503-2518.
- [24] A. Artemev, Y. Jin, A.G. Khachaturyan, Three-dimensional phase field model of proper martensitic transformation, *Acta. Mater.* 49 (2001) 1165-1177.
- [25] O.U. Salman, A. Finel, R. Delville, D. Schryvers, The role of phase compatibility in martensite, *J. Appl. Phys.* 111 (2012) 103517.
- [26] A. Artemev, J. Slutsker, A.L. Roytburd, Phase field modeling of self-assembling nanostructures in constrained films, *Acta. Mater.* 53 (2005) 3425-3432.

- [27] D.J. Seol, S.Y. Hu, Y.L. Li, L.Q. Chen, K.H. Oh, Computer simulation of martensitic transformation in constrained films, *Mater. Sci. Forum* 408-412 (2002) 1645-1650.
- [28] T.W. Heo, L.Q. Chen, Phase-field modeling of displacive phase transformations in elastically anisotropic and inhomogeneous polycrystals, *Acta. Mater.* 76 (2014) 68-81.
- [29] D. Fan, L.Q. Chen, Computer Simulation of Twin Formation during the Displacive $c \rightarrow t'$ Phase Transformation in the Zirconia-Yttria System, *J. Amer. Ceramic Soc.* 78 (1995) 769-773.
- [30] O. Shchyglo, G. Du, J.K. Engels, I. Steinbach, Phase-field simulation of martensite microstructure in low-carbon steel, *Acta Mater.* 175 (2019) 415-425.
- [31] O. Shchyglo, U. Salman, A. Finel, Martensitic phase transformations in Ni-Ti-based shape memory alloys: The Landau theory, *Acta Mater.* 60 (2012) 6784-6792.
- [32] A. Planes, P. Lloveras, T. Castán, A. Saxena, M. Porta, Ginzburg-Landau modelling of precursor nanoscale textures in ferroelastic materials, *Continuum Mech. Thermodyn.* 24 (2012) 619-627.
- [33] J. Kundin, D. Raabe, H. Emmerich, A phase-field model for incoherent martensitic transformations including plastic accommodation processes in the austenite, *J. Mech. Phys. Solids* 59 (2011) 2082-2102.
- [34] M. Mamivand, M.A. Zaeem, H.E. Kadiri, A review on phase field modeling of martensitic phase transformation, *Comput. Mater. Sci.* 77 (2013) 304-311.
- [35] V.I. Levitas, M. Javanbakht, Surface tension and energy in multivariant martensitic transformations: Phase-field theory, simulations, and model of coherent interface, *Phys. Rev. Lett.* 105 (2010) 165701.
- [36] A.Y. Woldman, C.M. Landis, Phase-field modeling of ferroelectric to paraelectric phase boundary structures in single-crystal barium titanate, *Smart Mater. Struct.*, 25 (2016) 035033.
- [37] V.I. Levitas, V.A. Levin, K.M. Zingerman, E.I. Freiman, Displacive phase transitions at large strains: Phase-field theory and simulations, *Phys. Rev. Lett.* 103 (2009) 025702.
- [38] V.I. Levitas, M. Javanbakht, Phase-field approach to martensitic phase transformations: Effect of martensite-martensite interface energy, *Int. J. Mater. Res.* 102 (2011) 652-665.
- [39] J.C.H. Lei, L.J. Li, Y.C. Shu, J.Y. Li, Austenite-martensite interface in shape memory alloys, *Appl. Phys. Lett.* 96 (2010) 141910.

- [40] F.E. Hildebrand, C. Miehe, A phase field model for the formation and evolution of martensitic laminate microstructure at finite strains, *Phil. Mag.* 92 (2012) 1-41.
- [41] J.D. Clayton, J. Knap, A phase field model of deformation twinning: Nonlinear theory and numerical simulations, *Physica D* 240 (2011a) 841-858.
- [42] J.D. Clayton, Nonlinear thermodynamic phase field theory with application to fracture and dynamic inelastic phenomena in ceramic polycrystals. *J. Mech. Phys. Solids* 157 (2021) 104633.
- [43] J.D. Clayton, J. Knap, Continuum modeling of twinning, amorphization, and fracture: theory and numerical simulations, *Continuum Mech. Thermodyn.* 30 (2018) 421-455.
- [44] H. She, Y. Liu, B. Wang, D. Ma Finite element simulation of phase field model for nanoscale martensitic transformation, *Comput. Mech.* 52 (2013) 949-958.
- [45] V.I. Levitas, D.L. Preston, Three-dimensional Landau theory for multivariant stress-induced martensitic phase transformations. I. Austenite \leftrightarrow Martensite, *Phys. Rev. B* 66 (2002) 134206.
- [46] V.I. Levitas, D.L. Preston, Three-dimensional Landau theory for multivariant stress-induced martensitic phase transformations. II. Multivariant phase transformations and stress-space analysis, *Phys. Rev. B* 66 (2002) 134207.
- [47] V.I. Levitas, Phase-field theory for martensitic phase transformations at large strains, *Int. J. Plast.* 49 (2013) 85-118.
- [48] V.I. Levitas, Phase field approach for stress- and temperature-induced phase transformations that satisfies lattice instability conditions. Part 1. General theory, *Int. J. Plast.* 106 (2018) 164-185.
- [49] H. Babaei, V.I. Levitas, Phase field approach for stress- and temperature-induced phase transformations that satisfies lattice instability conditions. Part 2. Simulations of phase transformations Si I \leftrightarrow Si II, *Int. J. Plast.* 107 (2018) 223-245.
- [50] K. Tůma, S. Stupkiewicz, Phase-field study of size-dependent morphology of austenite-twinned martensite interface in CuAlNi, *Int. J. Solids Struct.* 97-98 (2016) 89-100.
- [51] K. Tůma, S. Stupkiewicz, H. Petryk, Size effects in martensitic microstructures: Finite-strain phase field model versus sharp-interface approach, *J. Mech. Phys. Solids* 95 (2016) 284-307.
- [52] K. Tůma, S. Stupkiewicz, H. Petryk, Rate-independent dissipation in phase-field modelling of displacive transformations, *J. Mech. Phys. Solids* 114 (2018) 117-142.

- [53] M.R. Hajidehi, S. Stupkiewicz, Phase-field modeling of multivariant martensitic microstructures and size effects in nano-indentation, *Mech. Mater.* 141 (2020) 103267.
- [54] V.I. Levitas, A.V. Idesman, D.L. Preston, Microscale simulation of martensitic microstructure evolution, *Phys. Rev. Lett.* 93 (2004) 105701.
- [55] A.V. Idesman, V.I. Levitas, D.L. Preston, J.-Y. Cho, Finite element simulations of martensitic phase transitions and microstructure based on strain softening model, *J. Mech. Phys. Solids* 53 (2005) 495-523.
- [56] Levitas V.I., Esfahani S.E., and Ghamarian I. Scale-free modeling of coupled evolution of discrete dislocation bands and multivariant martensitic microstructure. *Phys. Rev. Lett.* 121 (2018) 205701.
- [57] Esfahani S.E., Ghamarian I., and Levitas V.I. Strain-induced multivariant martensitic transformations: A scale-independent simulation of interaction between localized shear bands and microstructure. *Acta Mater.* 196 (2020) 430-443.
- [58] Babaei H. and Levitas V.I. Finite-strain scale-free phase-field approach to multivariant martensitic phase transformations with stress-dependent effective thresholds. *J. Mech. Phys. Solids* 144 (2020) 104114.
- [59] V.I. Levitas, A.M. Roy, Multiphase phase field theory for temperature-induced phase transformations: Formulation and application to interfacial phases, *Acta Mater.* 105 (2016) 244-257.
- [60] V.I. Levitas, A.M. Roy, D.L. Preston, Multiple twinning and variant-variant transformations in martensite: Phase-field approach, *Phys. Rev. B* 88 (2013) 054113.
- [61] I. Steinbach, F. Pezzolla, B. Nestler, M. Seeßelberg, R. Prieler, G.J. Schmitz, J.L.L. Rezende. A phase field concept for multiphase systems, *Physica D.* 94 (1996) 135-147.
- [62] V.I. Levitas, A.M. Roy, Multiphase phase field theory for temperature- and stress-induced phase transformations, *Phys. Rev. B* 91 (2015) 174109.
- [63] J.Y. Cho, A.V. Idesman, V.I. Levitas, T. Park, Finite element simulations of dynamics of multivariant martensitic phase transitions based on Ginzburg-Landau theory, *Int. J. Solids Struct.* 49 (2012) 1973-1992.
- [64] Levin, V.A., Zingerman, K.M., 1998. Interaction and Microfracturing Pattern for Successive Origination (Introduction) of Pores in Elastic Bodies: Finite Deformation. *Trans. ASME. J. Appl. Mech.* 65, 431-435.

- [65] Levin, V.A., 1999. Multiple superposition of large deformation in elastic and viscoelastic bodies. Nauka, Moscow. (in Russian).
- [66] Levin, V.A., 1998. Theory of Repeated Superposition of Large Deformations. Elastic and Viscoelastic Bodies. *Int. J. Solids Struct.* 35, 2585-2600.
- [67] V.I. Levitas, Phase field approach to martensitic phase transformations with large strains and interface stresses, *J. Mech. Phys. Solids* 70 (2014) 154-189.
- [68] Levitas V.I. and Warren J. A. Phase field approach with anisotropic interface energy and interface stresses: large strain formulation. *J. Mech. Phys. Solids* 91 (2016) 94-125.
- [69] P.C. Bollada, P.K. Jimack, A.M. Mullis, Multiphase field modelling of alloy solidification, *Computat. Mater. Sci.* 171 (2020) 109085.
- [70] G.I. Tóth, T. Pusztai, L. Granasi, Consistent multiphase-field theory for interface driven multidomain dynamics, *Phys. Rev. B* 92 (2015) 184105.
- [71] C.S. Jog, *Continuum Mechanics: Foundations and Applications of Mechanics (Volume I)*, Cambridge Univ. Press, New Delhi, 2015.
- [72] I. Steinbach, Phase-field models in materials science, *Model. Simul. Mater. Sci. Eng.* 17 (2009) 073001.
- [73] A. Basak, V.I. Levitas, Finite element procedure and simulations for a multiphase phase field approach to martensitic phase transformations at large strains and with interfacial stresses. *Comput. Methods Appl. Mech. Engrg.* 343 (2019) 368–406.
- [74] W. Bangerth, D. Davydov, T. Heister, L. Heltai, G. Kanschat, M. Kronbichler, M. Maier, B. Turcksin, D. Wells, The deal.II library, version 8.4, *J. Numer. Math.* 24 (2016).
- [75] S.M. Ueland, C.A. Schuh, Grain boundary and triple junction constraints during martensitic transformation in shape memory alloys, *J. Appl. Phys.* 114(39) (2013) 053503.
- [76] A. Basak, V.I. Levitas, Interfacial stresses within boundary between martensitic variants: analytical and numerical finite strain solutions for three phase field models, *Acta Mater.* 139 (2017) 174-187.
- [77] Chen H., Levitas V.I., Popov D., and Velisavljevic N. Nontrivial nanostructure, stress relaxation mechanisms, and crystallography for pressure-induced Si-I \rightarrow Si-II phase transformation. *Nat. Commun.* 2022, DoI: 10.1038/s41467-022-28604-1.